Quaternary Science Reviews 312 (2023) 108168

Contents lists available at ScienceDirect

Quaternary Science Reviews

journal homepage: www.elsevier.com/locate/quascirev

Modelling of till microstructure development during subglacial deformation using ring shear experiments

Emrys Phillips [a, *], Jan A. Piotrowski [b, c]

[a] British Geological Survey, The Lyell Centre, Research Avenue South, Edinburgh, EH14 4AP, UK
[b] Department of Geoscience, Aarhus University, Høegh-Guldbergs Gade 2, 8000, Aarhus C, Denmark
[c] Faculty of Earth Sciences and Spatial Management, Nicolaus Copernicus University, Lwowska 1, 87-100, Toruń, Poland

ARTICLE INFO

Article history:
Received 1 March 2023
Received in revised form
22 May 2023
Accepted 2 June 2023
Available online 21 June 2023

Handling Editor: C. Ó Cofaigh

Keywords:
Ring shear experiments
Microstructural analysis
Simple shear
Subglacial shearing
Subglacial traction till

ABSTRACT

Micromorphology has become a principal tool in glacial sedimentology providing a wealth of data on the geometry and kinematics of deformation histories and aiding our understanding of progressive and polyphase deformation. This approach has been applied to the detailed microstructural analysis of fabric development in nine samples of experimentally deformed till subjected to simple shear in a ring shear apparatus in order to model the progressive microfabric development during simulated subglacial deformation. Thin section analysis revealed that the relative strength and complexity of the clast microfabrics increases with increasing cumulative shear distance (0–1152 cm) and cumulative shear strain (0–549), whereas microfabric strength increases rapidly during the initial stages of shearing (cumulative strain up to ~20) and remains relatively stable at higher cumulative strain (>200). In addition microfabric development is heterogeneous reflecting the partitioning of deformation at a microscale. A conjugate pattern of clast long axis alignment identified in the un-sheared sample taken at the start of the experiment formed during the initial consolidation and draining of the till. This emphasises that water-rich unconsolidated tills have the potential to be highly responsive to any applied stress even at very low strains. This un-sheared fabric was overprinted at a very early stage of the experiment when cumulative shear strains were below 5. The complex microfabrics formed during simple shear record the progressive development of up-shear dipping P-shears, down-shear dipping R-shears, and subhorizontal Y-shears. Sigmoidal fabric geometries, comparable to S–C and ECC-type fabrics, associated with the Riedel shears record a consistent sinistral sense of shear, i.e. the direction of shear imposed by the rotating plate of the ring shear. Observed changes in the relationships between these microfabrics record the switching between the localised imposition of a compressional fabric and P-shear formation, to subhorizontal shear and the formation of Y-shears accompanied by extension and the growth of low-angle R-shears, and back again. This process may potentially lead to alternating phases of "stick" (compression) and "slip" (subhorizontal shear) recognised as a key feature of glacier motion occurring in response to soft-sediment bed deformation. Multiple cycles of microstructure overprinting and rejuvenation pose a major challenge on determining the cumulative strain of subglacially deformed tills of unknown history from micromorphological signatures alone.

1. Introduction

Reconstructing the behaviour of past ice sheets and predicting the courses of future glaciations is to a large extent based on interpreting the properties of glacial deposits, in particular subglacial traction tills (Dreimanis, 1988; Menzies, 2002; Evans et al., 2006; Evans, 2018). Of special interest are tills left by highly dynamic ice streams (e.g. Jørgensen and Piotrowski, 2003; Spagnolo et al., 2016; Phillips et al., 2018b) which in-part regulated ice sheet mass balance and discharged of large volumes of ice at high rates (Stokes and Clark, 2001). Given the inaccessibility of modern subglacial environments, investigating tills generated at the now exposed ice-bed interfaces offers a wealth of proxies to constrain the glacier movement mechanisms, sediment transport and deposition, and the origin of certain active-ice landforms. The fast flow of ice streams may be facilitated by enhanced sliding along the

* Corresponding author.
E-mail address: erp@bgs.ac.uk (E. Phillips).

https://doi.org/10.1016/j.quascirev.2023.108168

ice-bed interface on a thin, discontinuous layer of pressurized meltwater at the bed surface that promotes slip effectively decouples ice from the substratum (Engelhardt and Kamb, 1998; Tulaczyk et al., 2000), by formation of a layer of soft, deforming till under the ice which carries the glacier forward (Alley et al., 1986; Blankenship et al., 1986), or any combination of these two processes giving rise to a mosaic of subglacial conditions transient in time and space (Piotrowski et al., 2004, 2006; Shumway and Iverson, 2009; Trommelen et al., 2012; Narloch et al., 2012; 2015; Tylmann et al., 2013; Schlegel et al., 2022). Identifying the specific processes from the past geological record is contentious (Piotrowski et al., 2001) but the impact of meltwater at the ice-bed interface on the mode of glacier movement is widely recognised (Hogan et al., 2022).

Using analogue laboratory experiments in a ring-shear apparatus (Fig. 1), this study investigates the evolution of micromorphological characteristics of a till subjected to progressively higher strains in an attempt to model the conditions occurring during subglacial deformation in the natural environment. The till comes from the bed of Odra Palaeo-Ice Stream (OPIS) at Kórnik south of Poznań in western Poland, an area located in the terminal part of the terrestrially-based Baltic Ice Stream Complex, which was active at the southern outskirts of the Scandinavian Ice Sheet during the last (Weichselian) glaciation (Punkari, 1997; Stokes and Clark, 2001; Przybylski, 2008; Szuman et al., 2021). The area comprises a field of low-relief mega-scale glacial lineations (MSGLs) with individual ridges up to ~4 m high, up to ~16 km long, and regularly spaced at 500–700 m crest-to-crest intervals. The Kórnik MSGLs were earlier investigated in detail by Spagnolo et al. (2016) and Phillips et al. (2018a, 2018b) with these studies focusing on their geological composition including micromorphological characteristics of undisturbed till samples. It was concluded that these MSGLs originated by time-transgressive accretion and streamlining of till under the fast-flowing ice. Till deposition was accompanied by ductile deformation in a thin layer of mobile sediment whereby the movement was partitioned into discrete, sequentially active microhorizons (décollement surfaces) softened by the migration of pressurized porewater.

The present study is a continuation of the work by Spagnolo et al. (2016) and Phillips et al. (2018b) with a focus on the rheological behaviour of the Kórnik till when subjected to shearing mimicking the response of subglacial traction till to the stresses

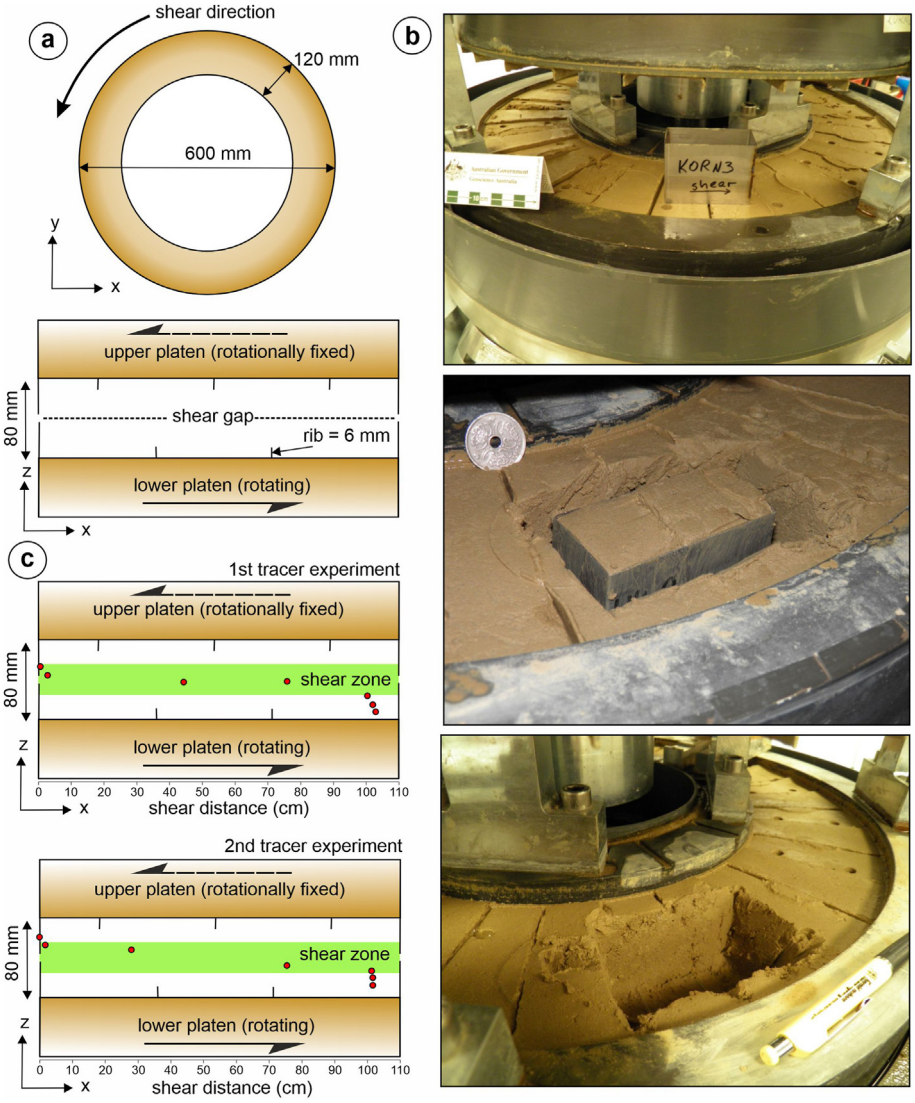

Fig. 1. (a) Schematic representation of the ring shear apparatus used in this study; **(b)** photographs of till sampling after one deformation increment (KORN3); and **(c)** the position of glass beads as tracers of strain after the shearing displacement of 100 cm before (upper panel) and after (lower panel) the main experiment (cf. Bering Holdensen, 2017).

imposed on it by the overriding glacier. Of particular interest was tracing the development of micromorphological signatures as a function of the increasing strain and relating these signatures to what was found in the original undisturbed till by the previous studies. The ultimate goal was to determine the possibility of using the micromorphological characteristics generated under controlled laboratory conditions as a reference to interpret the strain history of the natural subglacial traction tills, and scrutinize the implications of the results for deciphering the processes operating under soft-bedded glaciers and ice sheets.

2. Material and methods

2.1. The till

The Kórnik till used in the ring shear experiments is the sediment constituting the MSGLs generated by the OPIS. It forms a regionally extensive, at least 8-m thick till sheet composed of massive, matrix-supported, silty-sandy diamicton characterized by its remarkable textural and structural uniformity across the whole MSGLs field (Spagnolo et al., 2016). The grain-size fraction <2 mm consists of 62–71% sand, 29–38% silt and 4–9% clay. Gravel-sized clasts (2–64 mm) are rare and cobbles (>64 mm) extremely rare. Fine-gravel lithologies include sedimentary (e.g. siltstone, sandstone, mudstone, limestone), igneous (e.g. granite, altered volcanic rocks) and metamorphic rocks (e.g. amphibolite, biotite-schist) (see Table 1 of Phillips et al., 2018a, 2018b) sourced from the Scandinavian Shield and the Baltic Basin. No systematic trends in the distribution of grain sizes or lithological components occur in vertical profiles through the till. The *in-situ* clast macrofabric is well-developed and consistent with the elongation of the MSGLs (Spagnolo et al., 2016). Micromorphological analysis of undisturbed Kórnik till revealed that subglacial deformation resulted in complex systems of conjugate Riedel shears (P and R-shears) and a subhorizontal shear fabric (Y-shears) coplanar with the ice-bed interface and highlighted the lack of folding and/or faulting within the till (Phillips et al., 2018b).

The till used here was collected at sites A and B of Spagnolo et al. (2016) which are located along the crest of a prominent glacial lineation ridge in the central part of the Kórnik MSGL field. At both sites, the material was collected as bulk samples from below the soil horizon down to a depth of about 4 m, these were then mixed and subjected to further preparatory procedure in the laboratory (see below).

2.2. Ring shear experiments

Our knowledge of the conditions occurring beneath glaciers and ice sheets is limited primarily due to the extreme difficulty in accessing and observing modern subglacial environments. Consequently a number of studies have used ring-shear experiments to try and replicate these conditions within the laboratory, thereby enabling the modelling of the processes occurring during subglacial deformation and the mechanisms controlling glacier forward motion (e.g. Hooyer and Iverson, 2000; Hooyer et al., 2008; Iverson et al., 2008; Iverson and Zoet, 2015). For example, experiments conducted by Hooyer and Iverson (2000) demonstrated that during subglacial deformation clasts within a till will passively rotate into the shear plane and stay there, concluding that clast fabric strength reflects the magnitude of the imposed shear strains. Consequently, weak or spatially variable fabrics in tills which have not been strongly modified by later processes (periglacial, mass flow), indicate that the till has not been pervasively sheared to the high strains typically invoked by the deforming bed model of glacier forward motion (Iverson et al., 2008). Similar conclusions were reached by Thomason and Iverson (2006) and Larsen et al. (2006) who used orientations of microshears represented by grain lineations as a proxy of till strain generated in ring-shear experiments.

The ring-shear apparatus used in this study (Fig. 1) was previously applied to simulate subglacial sediment deformation and the related evolution of structural and textural characteristics of various diamictons and sorted granular materials (Larsen et al., 2006; Bateman et al., 2012, 2018; Damsgaard et al., 2013; Narloch et al., 2015). In the present setup (Fig. 1), the apparatus shears 14,480 cm^3 of sediment in an 8-cm deep and 12-cm wide chamber with an outer diameter of 60 cm at a constant rate of 2 mm/min and constant normal stress of 85 kPa. The applied normal stress is in the range of effective normal pressures beneath glaciers and ice sheets and the shearing velocity of around 1000 m/year is considered as realistic for fast-moving glaciers resting on a soft, deformable beds. Sediment shearing is achieved by rotating the lower platen under the fixed upper platen while ribs prohibit sliding between the sediment and the platens (Fig. 1a). The gap in the ring shear apparatus which accommodates the movement of the rotating lower platen, referred to as the shear gap, is located in the middle of the sample chamber (Fig. 1c). Water is allowed to enter and exit the sediment through filters in the lower and upper platen and through the gap between the platens. During shearing, changes in sediment thickness are recorded by three electronic transducers located at equal distances around the shearing chamber. The shear stress is measured by two transducers fixed on the opposite sides of the upper platen lid on its opposite sides across the shearing chamber. During the rotation of the lower platen, the

Table 1
Summary of microfabric data. E1 and E2 eigenvalues were calculated using the Principal Component Analysis (PCA) tools within StereoStat software by Rockworks ™ with data as lines (trend and plunge). N = number of measured clasts. An estimate of the relative strength of the microfabrics was made using the calculation spacing = length (L)/number of domains (N) (see Phillips et al., 2011 and references therein).

Sample	Cumulative shear distance (cm)	Cumulative shear strain (kPa)	relative microfabric strength (up-shear and down-shear combined)	N	E1	E2	Envelope of rose diagrams	
							Rf ratio	Orientation (φ)
KORN 0	0	0.0	10	4845	0.561	0.438	1.036	037.80
KORN 1	9	4.3	4.4	4828	0.613	0.386	1.445	147.24
KORN 2	18	8.6	1.9	4325	0.641	0.358	1.700	149.24
KORN 3	36	17.1	2.1	5457	0.635	0.364	1.607	147.95
KORN 4	72	34.3	2.1	3939	0.631	0.368	1.665	146.71
KORN 5	144	68.6	2.0	4738	0.652	0.347	1.792	147.32
KORN 6	288	137.1	1.6	4503	0.666	0.333	1.829	147.57
KORN 7	576	274.3	1.1	6245	0.672	0.327	1.812	142.32
KORN 8	1152	548.6	0.9	8240	0.687	0.312	1.813	150.30

transducers are pressed against stationary poles fixed to the ring-shear table outside the shearing chamber and thus record the shearing resistance generated in the sediment during shearing. Both, changes in the sediment thickness and in the shear stress are recorded in 30 s intervals.

Before inserting into the shearing chamber, the till was wetted to a water content of 17.9% (Bering Holdensen, 2017) making it a soft, easily deformable putty. The water content measured after the shearing experiment was 12.9% whereby the difference is attributed to water drainage from the till during its consolidation by normal load before each shearing increment and, to a lesser extent, during the shearing. After wetting, the till was fully remoulded to remove any pre-existing structural signatures. This was achieved by manual kneading, crumpling and squeezing of the till in a plastic container lasting about an hour to assure that each and every part of the material has been fully homogenized. Grains larger than 8 mm in diameter, which is one-tenth of the minimum dimension of the sample chamber, were removed according to standard conventions in soil science (Head, 1989). While placing the homogenized till in the shearing chamber, care was taken to prevent formation of any systematic fabric or layering, for example through smearing the till along the chamber or inserting it layer-by-layer. It is therefore assumed that the matrix microfabric was random at the start of experiment.

Prior to shearing, the sediment was subjected to 85 kPa normal stress for 1 h. During that time, the consolidation rate dropped exponentially so that at the end any remnant consolidation was negligible. The compacted sediment was sheared in eight successive runs of total shearing displacement of 9, 18, 36, 72, 144, 288, 576, and 1152 cm (Table 1). After each run, undisturbed samples were collected in aluminium Kubiena boxes (x = 8 cm, y = 6 cm, z = 4 cm) at the centreline of the chamber (Fig. 1b). The samples were numbered KORN 0 (before shearing) through KORN 8 (shearing displacement 1152 cm).

In order to determine the location of the main zone of sediment shearing and the cumulative strain, two experiments were conducted using glass beads as strain markers (see Fig. 1c), one before the main shearing experiment and another at the end (Bering Holdensen, 2017). In both cases, vertical columns of beads 3 mm in diameter were inserted into the till throughout its entire thickness and excavated after the shearing displacement of 100 cm. The shearing displacement divided by the thickness of the shear zone determined from the position of the displaced beads gives the value of sediment strain (Iverson et al., 1997). The averaged shear zone thickness measured after the two shearing displacements of 100 cm was used to calculate cumulative strain for each of the shearing increments KORN 0 through KORN 8 as above (Table 1).

2.3. Thin section and microstructural analysis

Over the past two decades micromorphology has become a principal tool in glacial sedimentology for distinguishing between subglacial and proglacial deformation. It has provided a wealth of data on the geometry and kinematics of deformation histories recorded by the diamictons deposited in these two settings (e.g. Menzies, 2000; Phillips and Auton, 2000; van der Wateren et al., 2000; Hiemstra and Rijsdijk, 2003; van der Meer et al., 2003; Menzies et al., 2006; Vaughan-Hirsch et al., 2013; Brumme, 2015; Gehrmann et al., 2017; Phillips et al., 2018a,b). Additionally, this type of analysis is being used with increasing success to aid our understanding of both progressive and polyphase deformation of glacigenic sequences (e.g. Phillips and Auton, 2000; van der Wateren et al., 2000; Phillips and Evans, 2019) as well as the role played by water during deformation (e.g. Hiemstra and van der Meer, 1997; Phillips and Auton, 2000; Khatwa and Tulaczyk, 2001; Baroni and Fasano, 2006; Phillips and Merritt, 2008; van der Meer et al., 2009; Phillips et al., 2013; 2018a; Phillips and Hughes, 2014; Phillips and Kearsey, 2020). Consequently, this approach has been applied in this study to the analysis of the deformation history imparted on the Kórnik till during the ring shear experiments.

Nine undisturbed samples (KORN 0 to 8) were collected (Fig. 1b) in order to investigate the progressive development of the microfabrics with increasing cumulative shear distance and strain (KORN 0 - cumulative shear distance = 0 cm; cumulative strain = 0, to KORN 8 - cumulative shear distance = 5760 cm; cumulative strain = 1152; Table 1). Sample preparation was carried out at Royal Holloway, University of London, using the methods outlined by Palmer (2005). Large format (10 × 8 cm), orientated thin sections were taken from the centre of each of the resin impregnated samples, avoiding artefacts associated with sample collection. Importantly, the thin sections were cut parallel to the shear direction and ensuring that they contain the principal stress directions imposed during the ring shear experiments. Consequently, the thin sections exhibit the most complete record of deformation and its intensity, and any kinematic indicators (e.g. asymmetrical folds, SC-fabrics … etc) can be correctly used to provide information on the evolution of the applied stress regime during the ring shear experiments. Initial analysis of the thin sections was carried out using a Zeiss petrological microscope revealing the composition, texture and structure of the sediment. Further detailed microscale analysis (Figs. 2–10) of the clast microfabrics developed

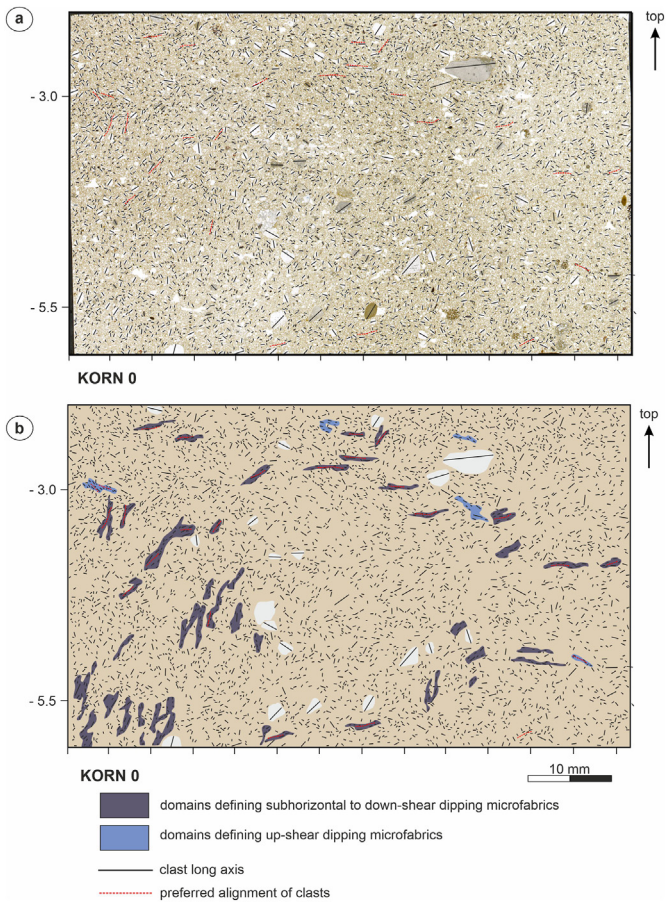

Fig. 2. Microstructural analysis of sample KORN 0: **(a)** High-resolution scan of the thin section with long axes of coarse-silt to small pebble sized clasts highlighted; and **(b)** map of the microfabrics developed in repose to deformation (see text for details).

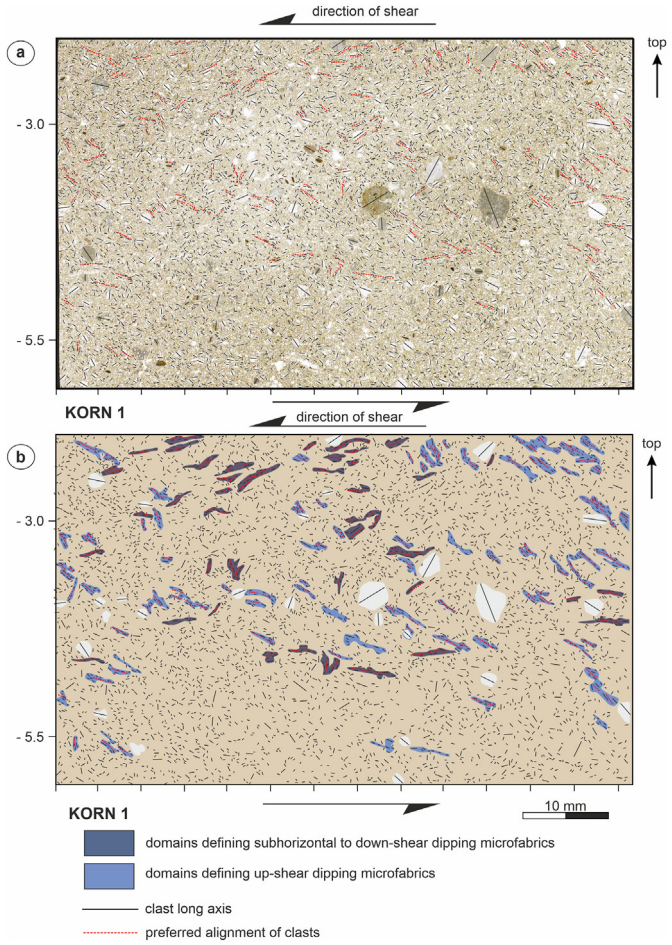

Fig. 3. Microstructural analysis of sample KORN 1: **(a)** High-resolution scan of the thin section with long axes of coarse-silt to small pebble sized clasts highlighted; and **(b)** map of the microfabrics developed in repose to deformation. Up-shear dipping clast microfabrics - pale blue domains; subhorizontal to gently down-ice dipping clast microfabrics – dark blue domains (see text for details).

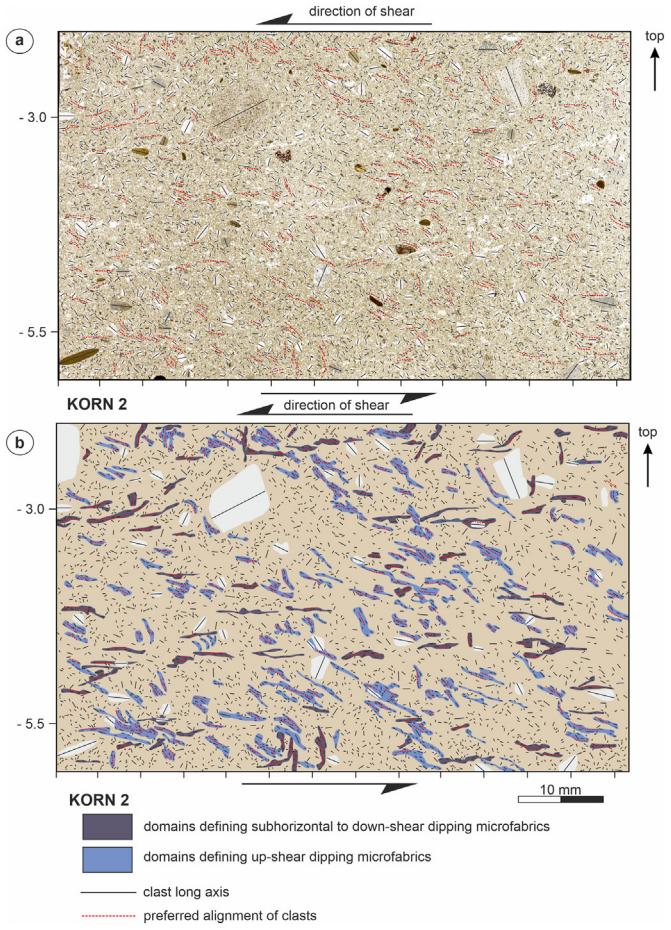

Fig. 4. Microstructural analysis of sample KORN 2: **(a)** High-resolution scan of the thin section with long axes of coarse-silt to small pebble sized clasts highlighted; and **(b)** map of the microfabrics developed in repose to deformation. Up-shear dipping clast microfabrics - pale blue domains; subhorizontal to gently down-ice dipping clast microfabrics – dark blue domains (see text for details).

within the experimentally deformed till was carried out using the methodology of Phillips et al. (2011). The method utilises high-resolution digital scans of the thin sections imported into a standard computer graphics package (e.g. CorelDraw®) to measure the orientation of long axes of detrital grains within the sediment. This process generates large 2D datasets (N = 4000–8000 grains; see Figs. 2–10, Table 1) with the clast orientation data for each sample being exported from CorelDraw into Excel as scalable vectors files (svg). The data are plotted on a series rose diagrams (Fig. 11) and the eigenvalues (E1, E2; Table 1) calculated for each sample using the commercial software package StereoStat by Rockware™.

The data are used to delineate the individual domains, composed of shape aligned elongate grains (coarse-silt up to small pebble-sized clasts), which define the clast microfabrics present within each sample (Figs. 2–10) defined by a preferred orientation of clastic grains and/or fabric elements (cf. Passchier and Trouw, 1996), and simply referred to here as either "fabric" or "microfabric". An estimate of the relative "strength" of the microfabric was made using two methods: the simple calculation of the number and spacing of the microfabric domains (spacing = length (L)/number of domains (N)); and calculating the E1 and E2 eigenvalues of the clast long axis data (Table 1) (see Phillips et al., 2011 and references therein). During this process, the relationships between successive generations of microfabrics are determined, allowing the relative chronology of fabric development (S1, S2, S3, Sn …. etc) to be established (see Phillips et al., 2011 for details). The results are used to construct a detailed model of microfabric development within the till during simple shear.

3. Results of ring shear experiments

Ring shear experiments run using the glass beads tracers reveal a well-defined main zone of shearing located approximately in the middle of the till coincident with the shearing gap between the upper and lower platens (Fig. 1a; Bering Holdensen, 2017). The relative displacement involved only two beads while the top two and bottom three beads remained essentially in place (non-displaced) indicating that the till had not been subjected to any significant intergranular advection. In the first experiment (100 cm of shearing freshly remoulded till), the shear zone had an estimated thickness of 1.8 cm, increasing to 2.4 cm thick in the second experiment (100 cm of shearing following the main shearing displacement of 1152 cm). These values give an average shear zone thickness of 2.1 cm which was used to calculate the cumulative strains, ranging from 0 (KORN 0) to 548.6 (KORN 8), after each successive run (Table 1). The shear stress curve resulting from the Kórnik ring shear experiments (Fig. 12) revealed an overall trend of shear stress increasing with strain, a feature typical for diamictic sediments; the initial values were around 16 kPa and rising to

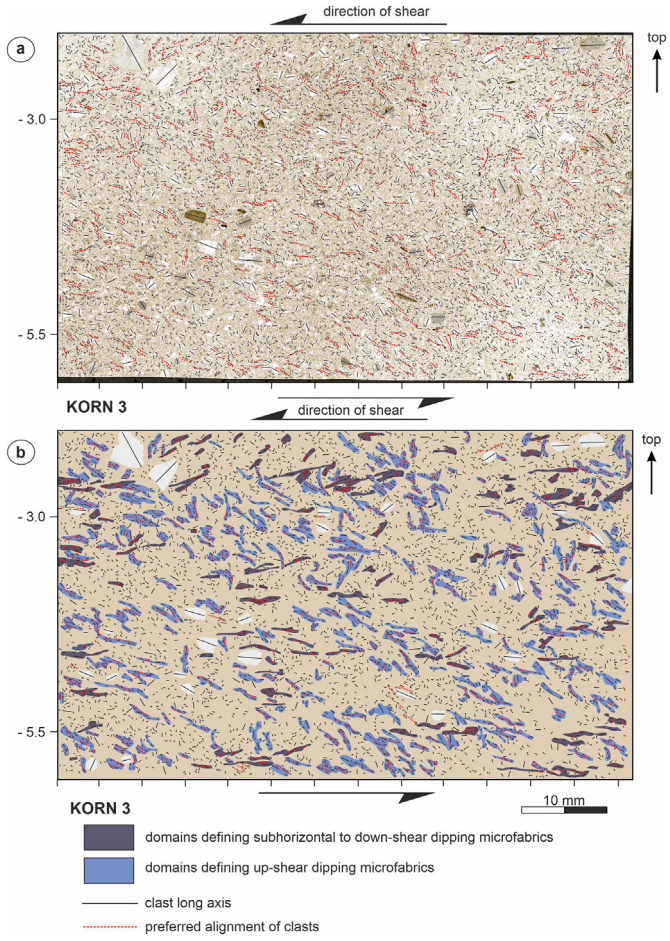

Fig. 5. Microstructural analysis of sample KORN 3: **(a)** High-resolution scan of the thin section with long axes of coarse-silt to small pebble sized clasts highlighted; and **(b)** map of the microfabrics developed in repose to deformation. Up-shear dipping clast microfabrics - pale blue domains; subhorizontal to gently down-ice dipping clast microfabrics – dark blue domains (see text for details).

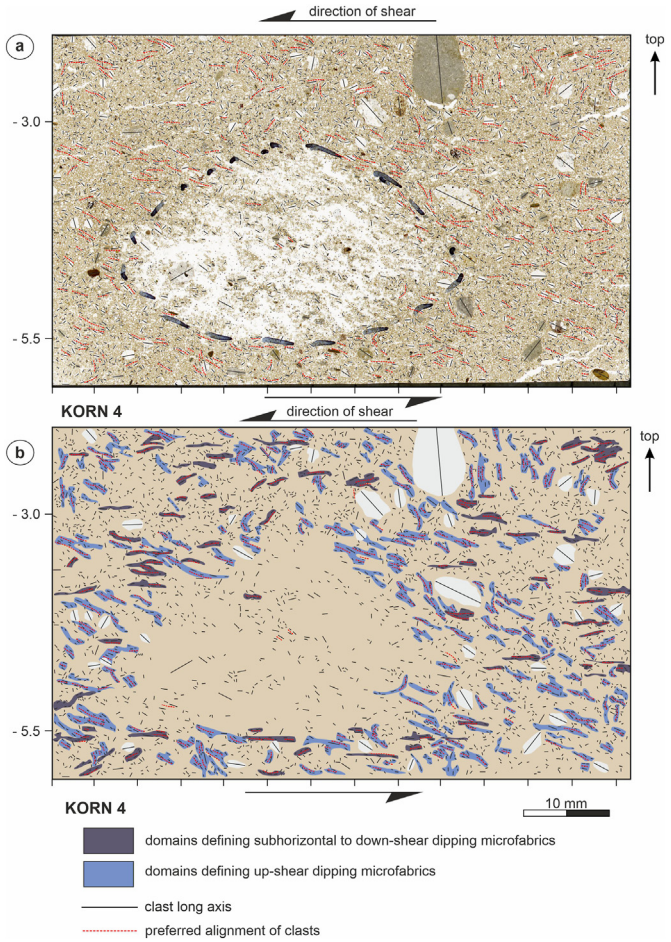

Fig. 6. Microstructural analysis of sample KORN 4: **(a)** High-resolution scan of the thin section with long axes of coarse-silt to small pebble sized clasts highlighted; and **(b)** map of the microfabrics developed in repose to deformation. Up-shear dipping clast microfabrics - pale blue domains; subhorizontal to gently down-ice dipping clast microfabrics – dark blue domains (see text for details). Black dashed line highlights area of thin section (centre of (a)) which was poorly impregnated resulting in removal of material during preparation.

around 54 kPa towards the end of experiment (Fig. 12a). After a shearing length of 500 cm, the curve displays characteristic cyclic fluctuations with an amplitude of ~7–~22 kPa. The specific mechanism of this cyclicity is contentious whereby an experimental artefact cannot be fully excluded, but it may be related to re-organization of the grain skeleton characterized by repeated build-up and failure of grain bridge networks mirrored in the phases of shear stress increase (the former) and drop (the latter). Similar quasi-periodic fluctuations were observed by Iverson et al. (1996) in their ring-shear experiments but these were normal-stress rather than shear-stress fluctuations measured here.

The tracer experiments clearly show that the strain is focused in a relatively narrow zone of shearing corresponding to about 26% of the entire sediment thickness. The lack of strain distribution through the whole sediment profile and, instead, its concentration along a prominent shearing horizon suggests that the till subjected to these specific boundary conditions behaves as a plastic (e.g. Iverson et al., 1998) and not viscous (Alley et al., 1986) material. Fluctuations in the normal stresses recorded during several previous studies (e.g. Iverson et al., 1996) has been potentially attributed to the repeated re-arrangement of the packing of the particles within the zone of shearing, such as the formation and collapse of grain stacks and bridges (Hooke and Iverson, 1995; Iverson et al., 1996; Larsen et al., 2007; Narloch et al., 2015). Once formed, these microstructures are considered to support most of the applied stress leading to its localized build-up, with the marked drop in shear stress observed during this study possibly occurring when these grain structures "fail" due to either intergranular slip, and/or grain crushing. This process would require the clasts to be in contact and would directly lead to a high proportion of fractured or broken grains within tills. However, although crushed grains do occur, their relative proportions tend to be rather low (e.g. table 2 of Carr et al., 2000, table 2 of Carr and Goddard, 2007, table 3 of van der Meer and Menzies, 2011; Narloch et al., 2020). In addition, the presence of intact, delicate shells (e.g. foraminifers, diatoms, thin-walled shells of molluscs) and/or undeformed soft-sediment intra clasts (mud intraclasts, till pebbles) in some tills have also been used as further evidence for the relatively low magnitude of the strains recorded by glacial sediments, including tills (e.g. Piotrowski et al., 2001). The regularity in the fluctuation in the shear stress curve resulting in wavelengths of around 45–50 cm indicates that whatever process is controlling this variation it is occurring repeatedly within the deforming till (see Section 5). The overall rise in shear stress during the ring shear experiment could potentially be attributed to gradual stiffening of the till either due to dilatant/strain hardening of the sediment (Moore and Iverson,

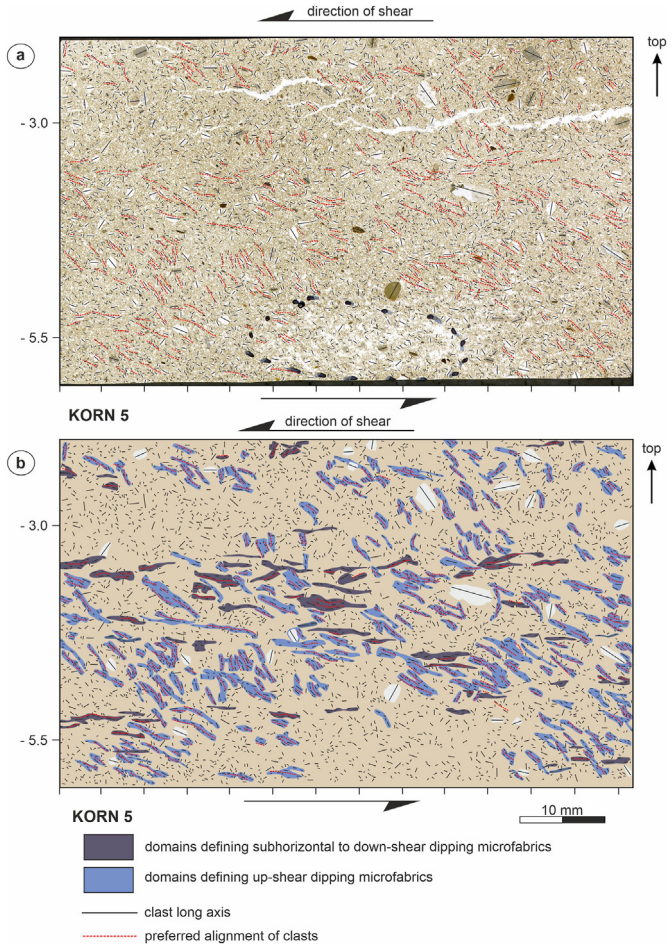

Fig. 7. Microstructural analysis of sample KORN 5: **(a)** High-resolution scan of the thin section with long axes of coarse-silt to small pebble sized clasts highlighted; and **(b)** Map of the microfabrics developed in repose to deformation. Up-shear dipping clast microfabrics - pale blue domains; subhorizontal to gently down-ice dipping clast microfabrics – dark blue domains (see text for details). Black dashed line highlights area of thin section (lower part of (a)) which was poorly impregnated resulting in removal of material during preparation.

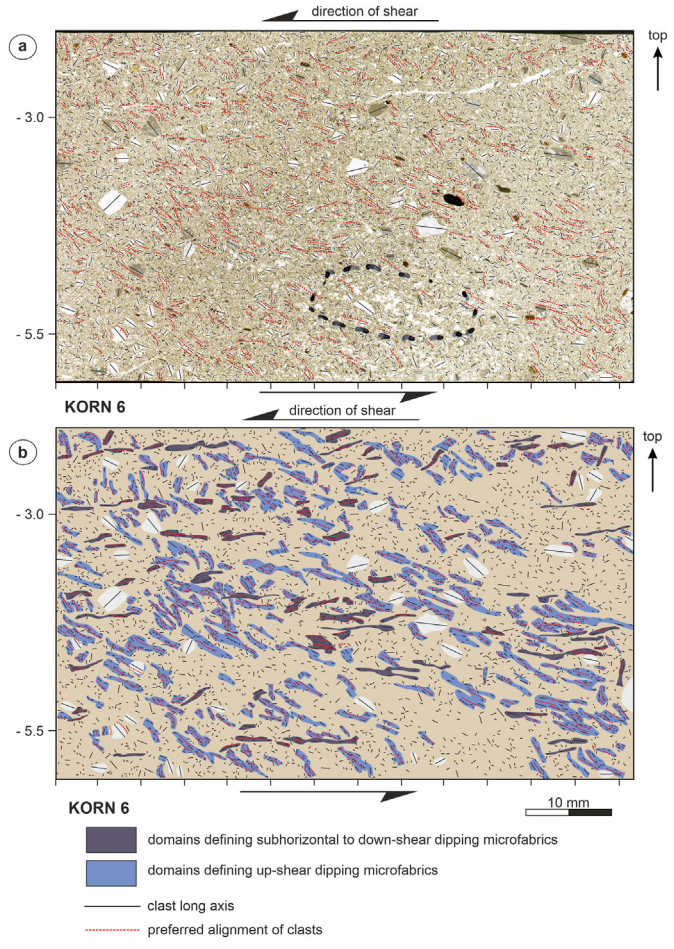

Fig. 8. Microstructural analysis of sample KORN 6: **(a)** High-resolution scan of the thin section with long axes of coarse-silt to small pebble sized clasts highlighted; and **(b)** map of the microfabrics developed in repose to deformation. Up-shear dipping clast microfabrics - pale blue domains; subhorizontal to gently down-ice dipping clast microfabrics – dark blue domains (see text for details). Black dashed line highlights area of thin section (lower part of (a)) which was poorly impregnated resulting in removal of material during preparation.

2002; Iverson, 2010; Damsgaard et al., 2015) or porewater escaping through the filters and the shearing gap between the platens (i.e. sediment dewatering).

4. Results of microstructural analysis

4.1. Microfabrics developed in response to simple shear

Analysis of thin sections KORN 0 to KORN 8 has revealed that the relative strength (Table 1) and complexity of the microfabrics within the experimentally deformed till increases with increasing cumulative shear displacement and shear strain (Figs. 2–10). These changes are summarised in Fig. 11, which also includes a series of rose diagrams showing the variation in clast long axis orientation and orientation of the dominant microfabrics. The geometry of these microfabrics is consistent with deformation being dominated by sinistral (top-to-left) simple shear induced by the rotation of the lower platen of the ring shear (see Fig. 1a). Two main clast microfabrics have been recognised: (i) a moderately (~30–40°) up-shear dipping, discontinuous, spaced microfabric defined by relatively short, irregular to S-shaped (sigmoidal) domains (pale blue on Figs. 3–10); and (ii) a subhorizontal to gently (<10–20°) down-shear dipping, discontinuous, spaced microfabric defined by short, irregular to more elongate planar domains (dark blue on Figs. 3–10) (for the terminology used to describe the microfabrics see Fig. 4 of Phillips et al., 2011). The increase in relative strength of these microfabrics from sample KORN 3 through to KORN 8 (Fig. 11) is reflected in an increase in both the number and length of the microfabric domains, accompanied by a decrease in their spacing (compare Figs. 5 and 10). Microfabric strength also varies within an individual thin section reflecting the heterogeneous nature of fabric development and the partitioning of deformation within the till (Figs. 4, 5, 7 and 8). In addition, the spacing of the microfabric domains may also be locally governed by the presence of larger clasts (Figs. 4–6 and 9).

KORN 0 (Fig. 2) represents the starting material prior to shearing and was therefore considered “undeformed”. However, although poorly developed, two clast microfabrics can be recognised: (i) a steeply dipping to subvertical fabric (pale blue domains on Fig. 2) which is most obvious in the lower left-hand side of the thin section; and (ii) a poorly developed subhorizontal microfabric (dark blue on Fig. 2). Furthermore, when plotted on a rose diagram the clast long axis orientation data reveals a distinct “bow-tie” or conjugate pattern (green arrows on Fig. 11a) as well as preferred subhorizontal clast alignment. This conjugate pattern is also

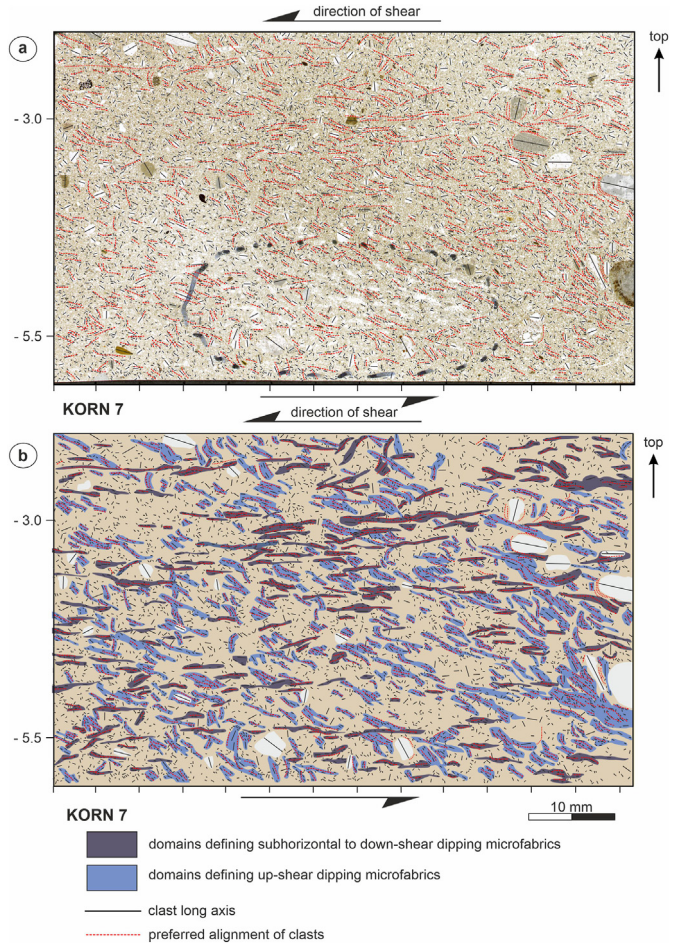

Fig. 9. Microstructural analysis of sample KORN 7: **(a)** High-resolution scan of the thin section with long axes of coarse-silt to small pebble sized clasts highlighted; and **(b)** map of the microfabrics developed in repose to deformation. Up-shear dipping clast microfabrics - pale blue domains; subhorizontal to gently down-ice dipping clast microfabrics – dark blue domains (see text for details). Black dashed line highlights area of thin section (lower part of (a)) which was poorly impregnated resulting in removal of material during preparation.

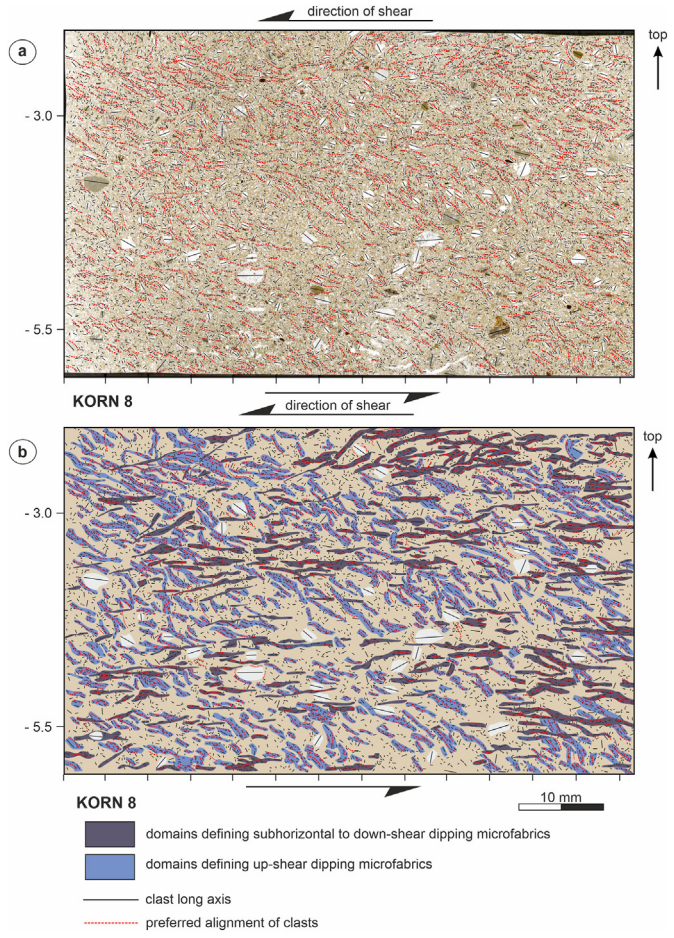

Fig. 10. Microstructural analysis of sample KORN 8: **(a)** High-resolution scan of the thin section with long axes of coarse-silt to small pebble sized clasts highlighted; and **(b)** map of the microfabrics developed in repose to deformation. Up-shear dipping clast microfabrics - pale blue domains; subhorizontal to gently down-ice dipping clast microfabrics – dark blue domains (see text for details).

apparent in KORN 1 (Fig. 11b) but is absent within KORN 2 to 8 (Fig. 11c–i) indicating that this feature became progressively overprinted during simple shear (cumulative shear strains of ≥8.5; Table 1).

The observed increase in microfabric development in samples KORN 1, 2 and 3 (Figs. 3–5, 11) corresponds to an increase in cumulative shear strain from 4.3 to 17.1 (Table 1). The dominant fabric is a heterogeneously developed up-shear dipping microfabric and is represented by a marked elliptical pattern of the data displayed on the rose diagrams (Fig. 11c and d). Microfabric development was initiated within the upper part of KORN 1 (Fig. 3) close to the fixed, upper platen of the ring shear, progressively moving down through sample KORN 2 (Fig. 4), becoming more widely developed in KORN 3 (Fig. 5). In KORN 2 and 3 this fabric comprises two discrete components: (i) a moderate to shallow dipping (≤30–45°) fabric (Fig. 11c and d) locally defining discrete bands of relatively more intense fabric development (KORN 3, Fig. 5); and (ii) a weak heterogeneous developed, more steeply dipping component.

The relationship(s) between the up-shear dipping fabric and the weaker subhorizontal microfabric varies both between samples (Fig. 11) and within a single thin section (Figs. 3 and 4) leading to difficulties in establishing the temporal relationships (S1, S2, S3, …. etc) between these fabrics. In KORN 2 the subhorizontal fabric forms narrow, laterally extensive bands (apparent relative age S2) which typically crosscut the earlier developed up-shear dipping fabric (apparent relative age S1), the latter being preserved as straight to sigmoidal (S-shaped) domains within the microlithons separating the subhorizontal microfabric (Fig. 4). However, in the lower left-hand corner and central upper part of the same thin section the opposite relationship occurs (see Fig. 4) (subhorizontal fabric = S1, up-shear dipping fabric = S2). The complex cross-cutting relationships between the two dominant microfabrics is also apparent within the remaining samples (Figs. 5–10) which record an increase in cumulative shear strain from 17.1 to 548.6 (Table 1). In KORN 3 to KORN 8 the subhorizontal to gently down-shear dipping microfabrics (apparent relative age S2) form increasingly laterally persistent bands which crosscut and deform the apparently earlier up-shear dipping fabric (apparent relative age S1), the latter being defined by straight to sigmodal domains which record a consistent sinistral (top-to-left) sense of shear (Figs. 13 and 14). These relationships are most apparent in samples KORN 5 to KORN 8 (Figs. 7–10) where they record the progressive development of subhorizontal sinistral shear zones and the associated intensification/strengthening of the associated microfabrics (Figs. 10, 13 and 14). These shear zones were initially preferentially developed in the central to lower part of the till (KORN 5; Fig. 7),

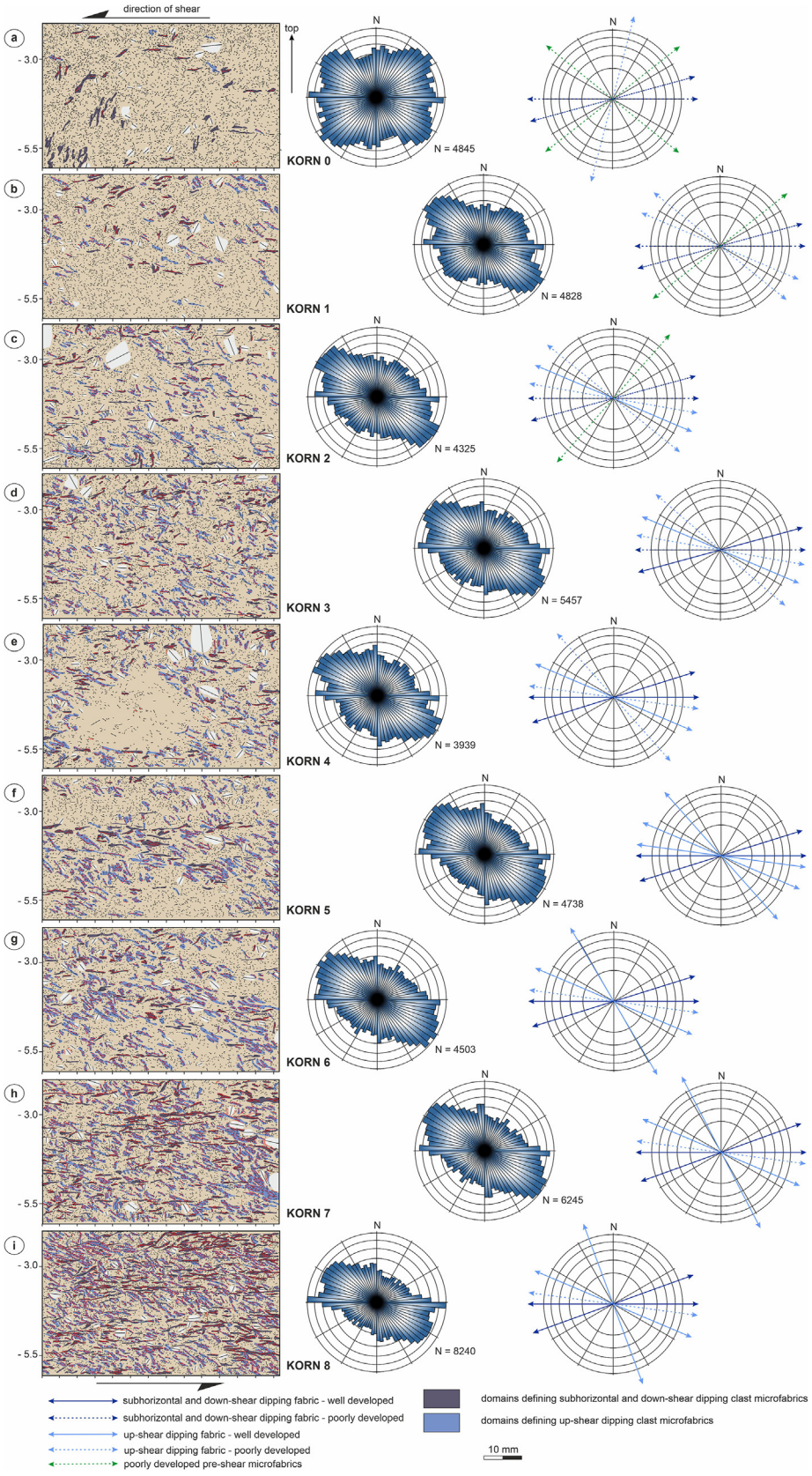

Fig. 11. Microstructural maps and rose diagrams (N = number of clasts) showing the variation in microfabric development within samples: **(a)** KORN 0; **(b)** KORN 1; **(c)** KORN 2; **(d)** KORN 3; **(e)** KORN 4; **(f)** KORN 5; **(g)** KORN 6; **(h)** KORN 7; and **(i)** KORN 8.

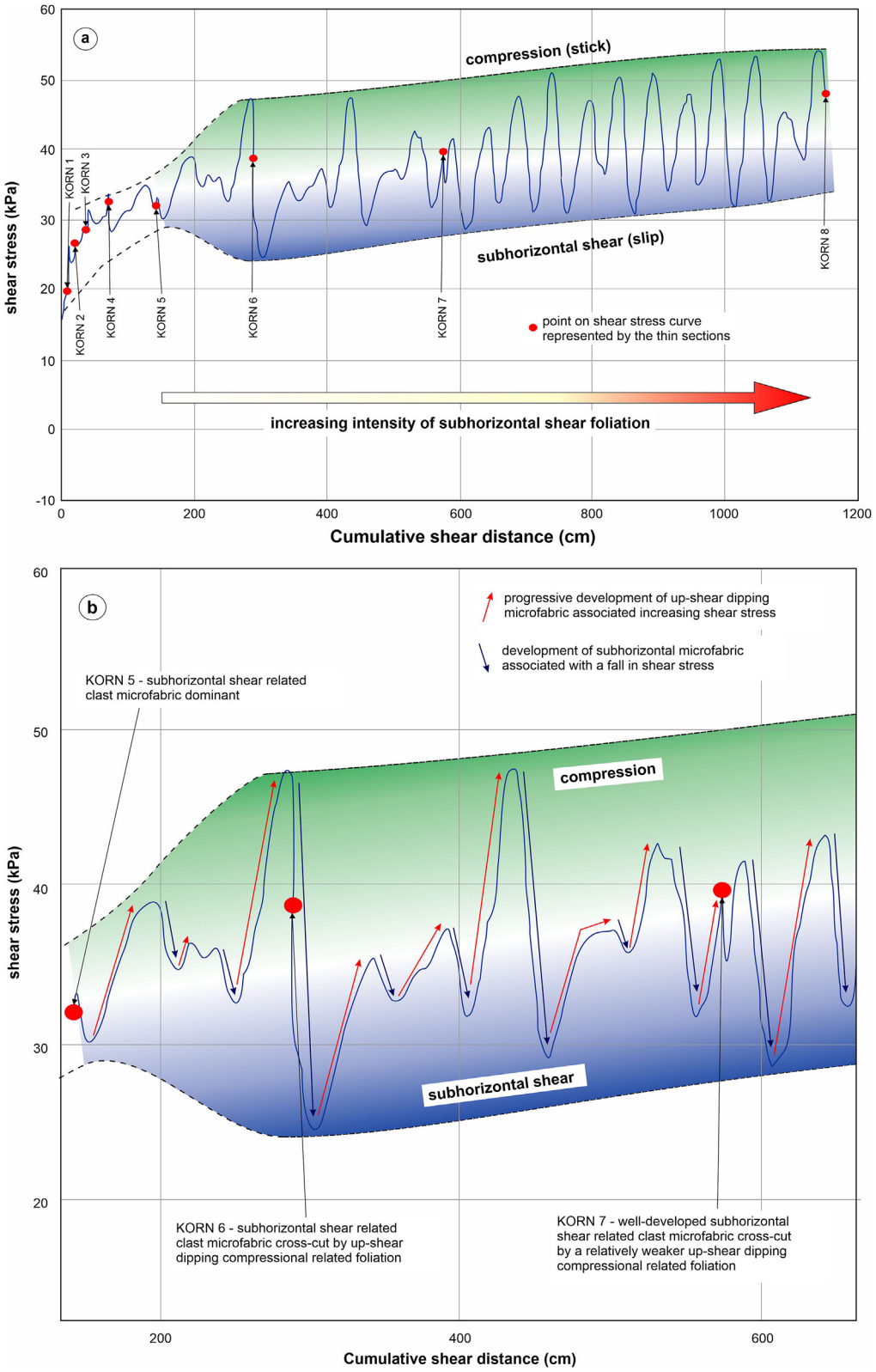

Fig. 12. (a) Graph showing the variation in shear stress (kPa) versus cumulative shear distance (cm) and the relationship between microfabric development due to compression (stick) and subhorizontal shear (slip) with respect to changes within the shear stress curve. Also shown are the points at which samples KORN 0 to 8 were taken during the ring shear experiment; and **(b)** enlargement of part of the shear stress curve highlighting the parts of the curve relating to the progressive development of the up-shear dipping microfabric and subhorizontal microfabric (see text for details).

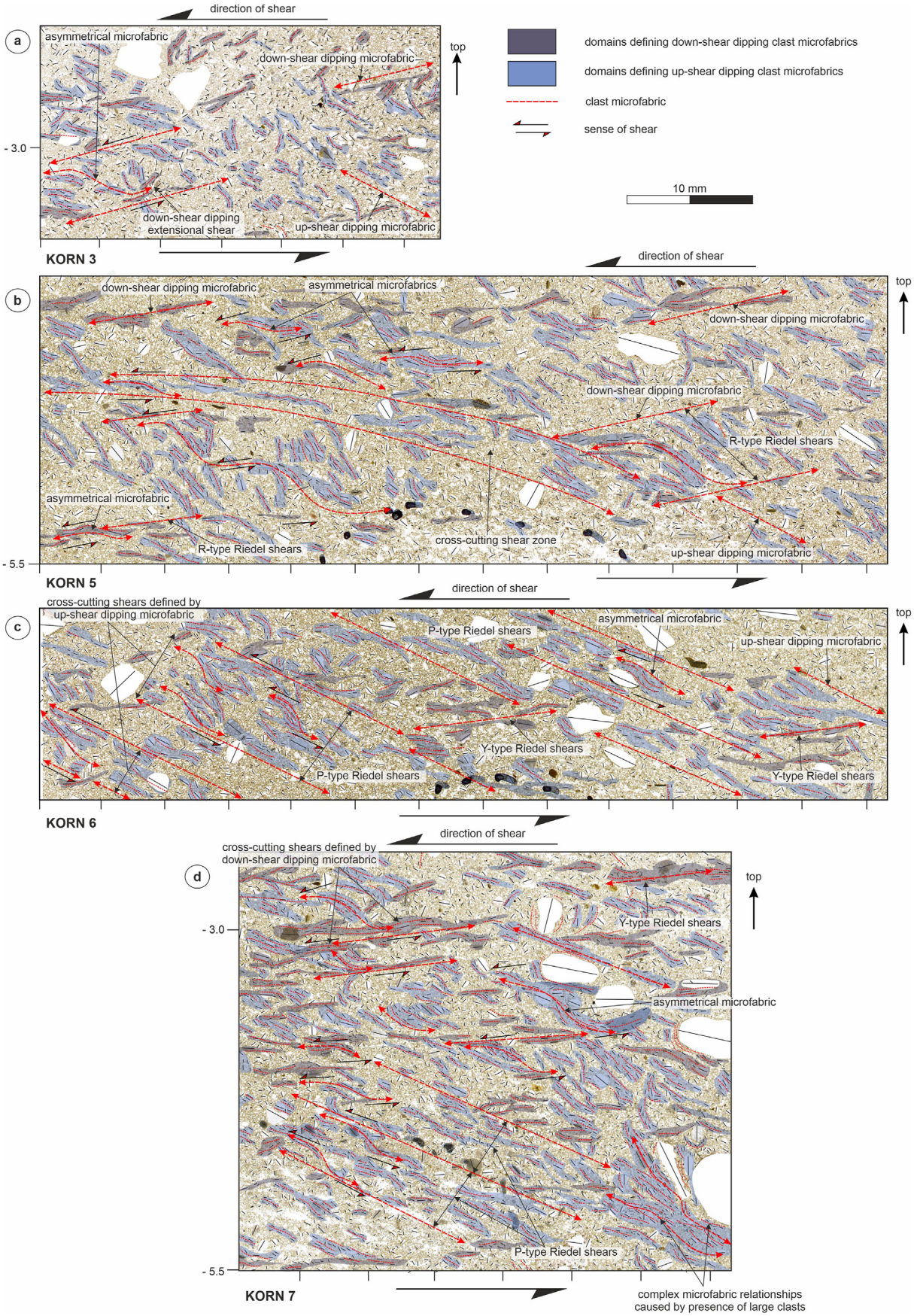
a
direction of shear
asymmetrical microfabric
down-shear dipping microfabric
top
- 3.0
down-shear dipping extensional shear
up-shear dipping microfabric
KORN 3
domains defining down-shear dipping clast microfabrics
domains defining up-shear dipping clast microfabrics
clast microfabric
sense of shear
10 mm
b
direction of shear
down-shear dipping microfabric
asymmetrical microfabrics
top
down-shear dipping microfabric
down-shear dipping microfabric
R-type Riedel shears
asymmetrical microfabric
R-type Riedel shears
cross-cutting shear zone
up-shear dipping microfabric
- 5.5
KORN 5
c
direction of shear
cross-cutting shears defined by up-shear dipping microfabric
P-type Riedel shears
asymmetrical microfabric
top
up-shear dipping microfabric
Y-type Riedel shears
P-type Riedel shears
Y-type Riedel shears
KORN 6
direction of shear
d
cross-cutting shears defined by down-shear dipping microfabric
top
- 3.0
Y-type Riedel shears
asymmetrical microfabric
P-type Riedel shears
- 5.5
KORN 7
complex microfabric relationships caused by presence of large clasts

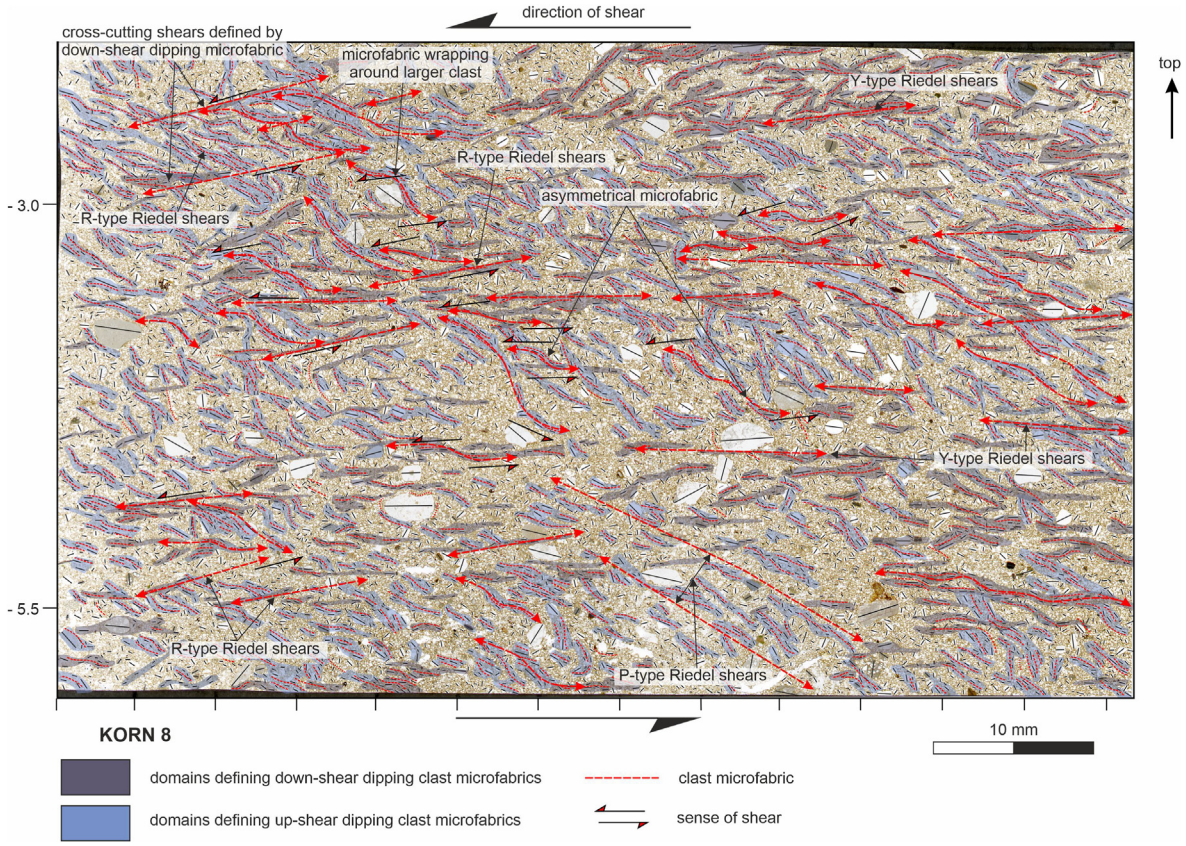

Fig. 14. Structural interpretation of the microfabrics developed within part of sample KORN 8 showing the complex fabric relationships associated with the development of subhorizontal Y-type shears, down-shear dipping R-type shears and up-shear dipping P-type Reidel shears (see text for details).

becoming more pervasively developed throughout the till (KORN 7 and 8; Figs. 9 and 10, respectively) as the cumulative shear strains increased.

In KORN 3, 6 and 7 (Figs. 5, 8 and 9, respectively) the subhorizontal shears are crosscut by narrow, moderately dipping (~30°) bands of the up-shear dipping fabric which clearly post-date the formation of the shear zones (Fig. 13b, c, d). Where these bands of up-shear dipping fabric are better developed (KORN 6; Fig. 8) they comprise straight to sigmoidal domains once again recording a sinistral sense of shear (Fig. 13c and d). In contrast, in KORN 4, 8 and to a lesser extent 5 (Figs. 6, 7 and 10, respectively) the cross-cutting bands of up-shear dipping fabric are either absent or very weakly developed (Fig.. 13b and 14).

4.2. Variation in microfabric strength

E1 and E2 eigenvalues were calculated for all the samples in order to quantify the progressive increase in microfabric strength (Table 1) and are plotted against cumulative shear distance and cumulative shear strain on Fig. 15. The initially steep gradient of the curve defined by the data records a marked rise in E1 (KORN 0, E1 = 0.561 to KORN 3, E1 = 0.635) equating to the early stages of microfabric development at low cumulative strains (≤20). This initial phase was followed by a more gradual increase in microfabric strength (KORN 4, E1 = 0.631 to KORN 8, E1 = 0.687) and its apparent stabilisation at higher cumulative strains (≥200 kPa) (Table 1; Fig. 15). Thomason and Iverson (2006) and Hooyer et al. (2008) described a similar pattern of initially rapidly increasing eigenvalues followed by a more stable to gradual increase with increasing shear strain characterised the progressive development of clast and AMS (magnetic) fabrics in the experimentally deformed Douglas and Batestown tills. Although KORN 0 was collected prior to the start of the ring shear experiment and therefore "undeformed", the calculated E1 value (E1 = 0.561) does not correspond to a fully distributed orientations reflecting the distinct conjugate pattern within the clast data (Fig. 11a). This conjugate microfabric is considered to have formed in response to the initial consolidation and dewatering of the till prior to starting the ring shear experiment. Comparable microfabric strengths formed prior to shearing were reported by Thomason and Iverson (2006) who similarly interpreted the data as recording initial consolidation of the till and/or incomplete mixing of the sample prior to consolidation.

An alternative method for quantifying the progressive microfabric development involves the calculation of the Rf ratio of an ellipse (Rf = short axis/long axis) enclosing the clast orientation data plotted on the rose diagrams (Fig. 16a); a circle (Rf = 1)

Fig. 13. (a) Structural interpretation of the microfabrics developed within part of sample KORN 3 showing the asymmetrical fabrics developed within a down-shear dipping R-type Reidel shear; **(b)** structural interpretation of the microfabrics developed within part of sample KORN 5 showing the asymmetrical fabrics developed within the well-developed down-shear dipping R-type Reidel shears. These shears are crosscut by a narrow band of up-shear dipping fabric defining a P-type Reidel shear; **(c)** structural interpretation of the microfabrics developed within part of sample KORN 6 showing the asymmetrical fabrics developed within a set of well-developed up-shear dipping P-type Reidel shears; and **(d)** structural interpretation of the microfabrics developed within part of sample KORN 7 showing the complex fabric relationships associated with the development of subhorizontal Y-type Reidel shears and up-shear dipping P-type shears (see text for details).

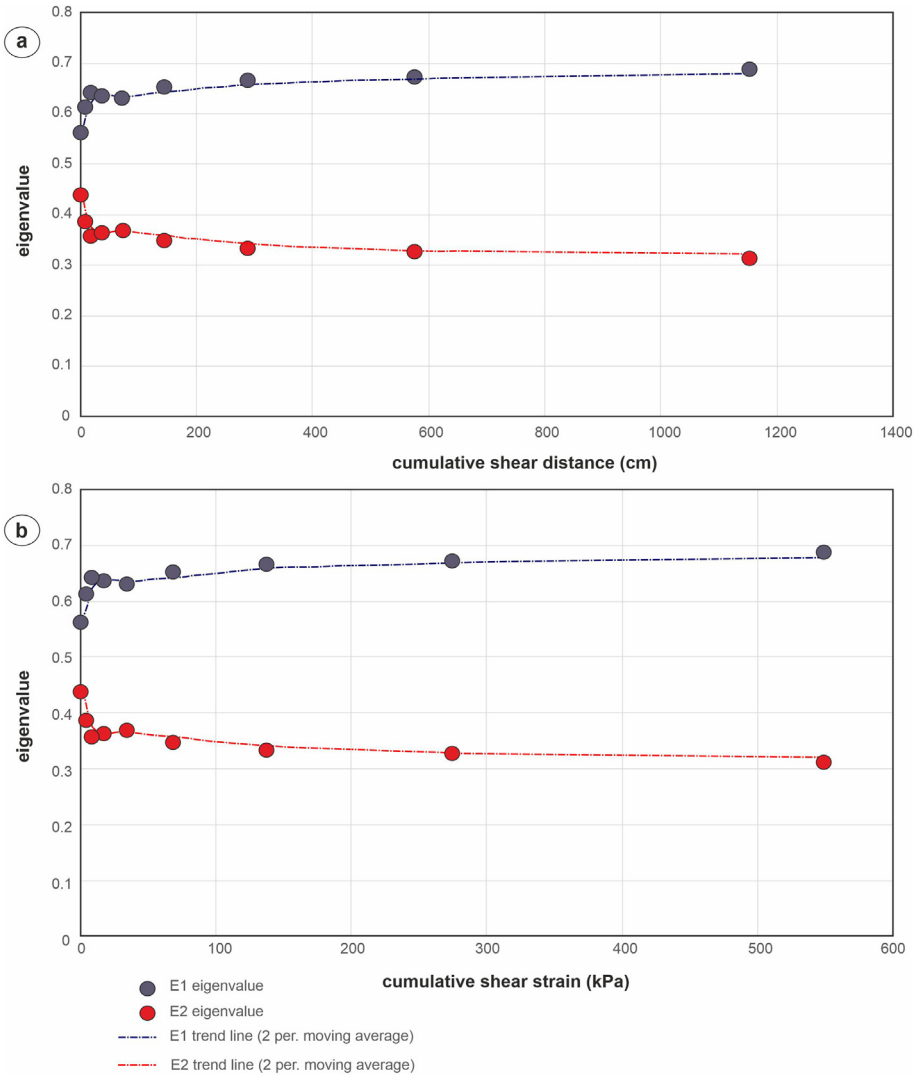

Fig. 15. Graphs showing the variation in E1 and E2 eigenvalues versus **(a)** cumulative shear distance (cm) and **(b)** cumulative shear strain reflecting the variation in microfabric strength during the ring shear experiment.

corresponds to a random arrangement (i.e. no microfabric), with a more elongate ellipse (Rf > 1) recording a progressive increase in microfabric strength. The calculated Rf values range between 1.04 (KORN 0) and 1.833 (KORN 6) (Fig. 16a; Table 1) and define a distinct curve on Fig. 16b, once again reflecting initially rapid microfabric development at low strains (<20 kPa), followed by a more gradual increase and apparent stabilisation of fabric strength (Rf = 1.83–1.81) at higher cumulative shear strains (>200).

Both methods clearly record the progressive increase in microfabric strength during initial stages of shearing and produce curves comparable to those for the Douglas and Batestown tills published by Thomason and Iverson (2006). However, the thin sections of the Kórnik till used in this study clearly show that microfabric development is heterogeneous reflecting the partitioning of deformation at a microscale during simple shear (Fig. 14). In order to quantify this variation each thin section was divided into 28 (1 cm × 1 cm) areas and the eigenvalues calculated for each subset of the clast data. The results are shown on Fig. 17; purple colours representing low fabric strengths (E1 = 0.51–0.58), green colours moderate strength fabrics (E1 = 0.58–0.69), and yellow to red, the highest fabric strengths (E1 = 0.69–0.80). This reveals that fabric strength not only varies within an individual thin section, but also clearly shows the progressive increase in microfabric strength in response to increased cumulative strain. In samples KORN 0, 1 and 2 the relatively higher fabric strengths occur in the upper to central part of the thin section suggesting that fabric development was initially concentrated in that part of the till (Fig. 17a–c). However, in KORN 3 to 8 this pattern is reversed with the higher microfabric strengths occurring lower in the sample (Fig. 17d–i) with the highest E1 values typically coinciding within the shear zone determined from the position of the displaced glass beads (see Fig. 1a).

5. Interpretation of microstructural analysis: microfabric development in response to progressive ductile simple shear

Microstructural analysis clearly reveals that even prior to the start of the ring shear experiment microfabric development had commenced within the Kórnik till (KORN 0) (Fig.. 11a and 17a). This conjugate fabric is considered to have formed during the initial consolidation and draining of the till emphasising that water-rich unconsolidated sediments have the potential to be highly responsive to any applied stress even at very low strains (Fig.. 15b and 17a). This microfabric is recognised in samples KORN 0 and 1, but is absent in KORN 2 (Fig. 11a–c and 17a to c) indicating that this

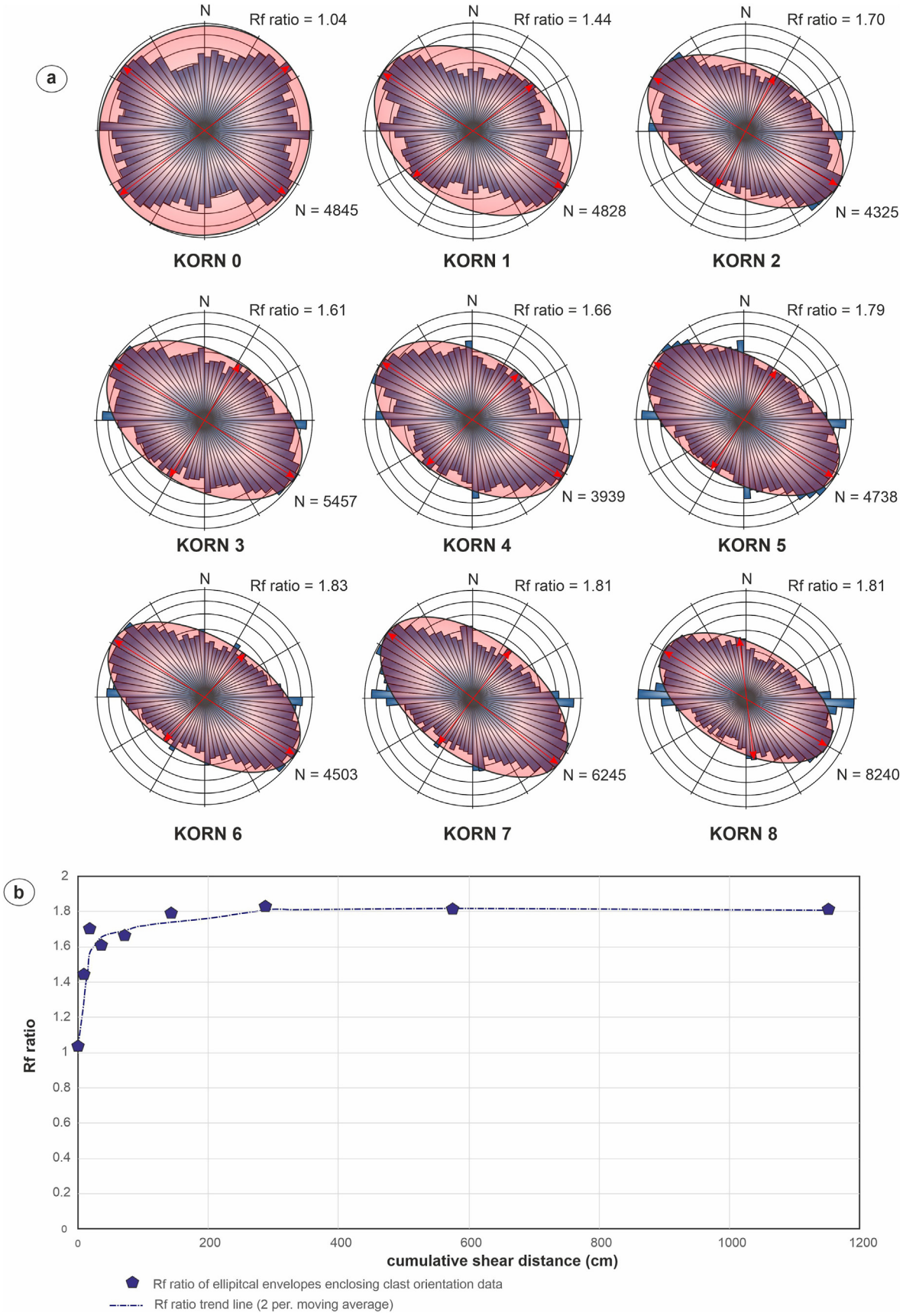

Fig. 16. (a) Rose diagrams showing variation in clast long axis orientation in samples KORN 0 to 8 and the Rf ratio (Rf = long axis/short axis) of the ellipse enclosing the data; and **(b)** plot of Rf ratio versus cumulative shear distance showing the variation in microfabric strength during the ring shear experiments.

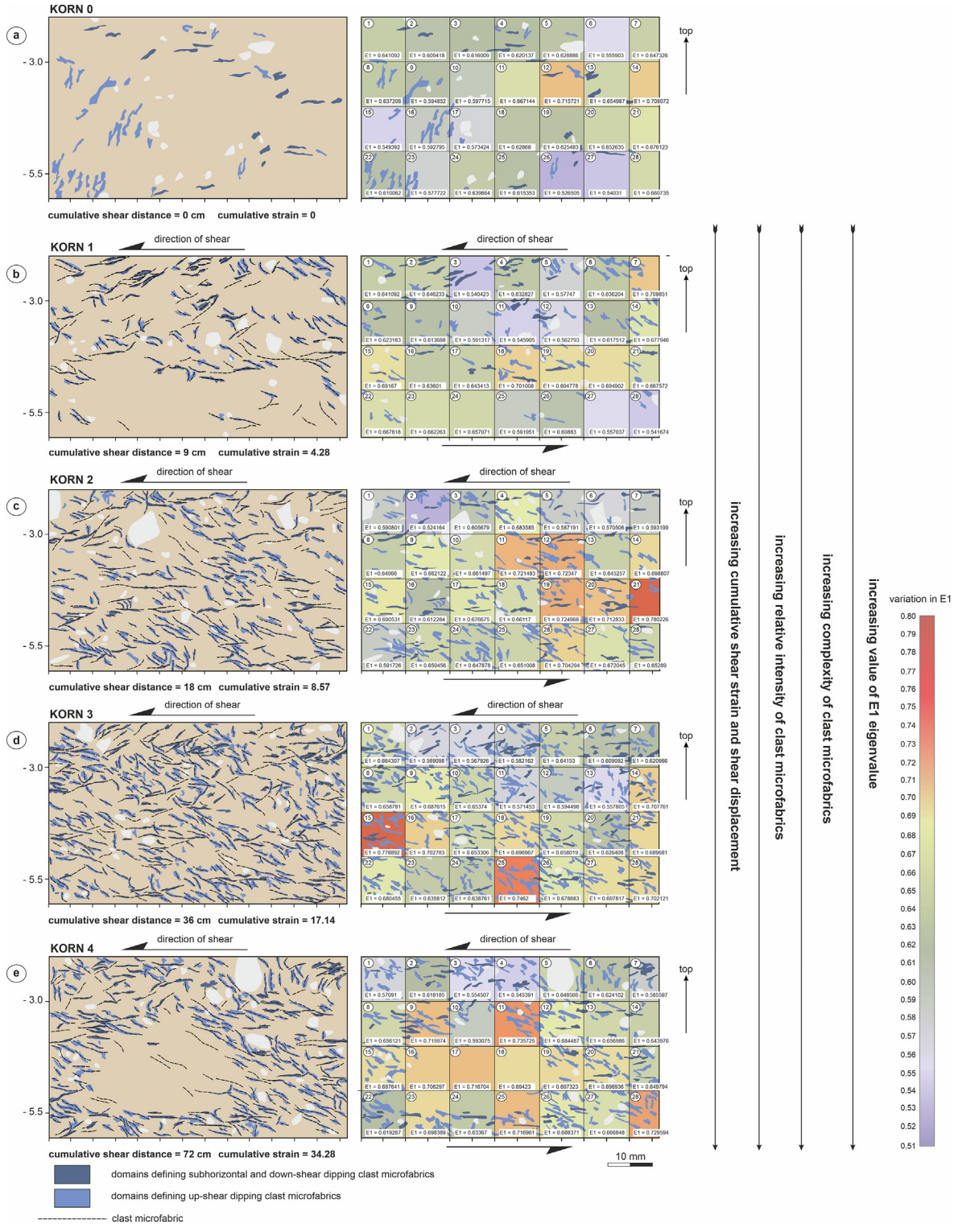

Fig. 17. Diagram showing the variation in clast microfabrics and calculated (E1 eigenvalue) microfabric strength derived from the detailed microstructural analysis of the thin sections: **(a)** KORN 0; **(b)** KORN 1; **(c)** KORN 2; **(d)** KORN 3; **(e)** KORN 4; **(f)** KORN 5; **(g)** KORN 6; **(h)** KORN 7; and **(i)** KORN 8.

consolidation related fabric was overprinted at a very early stage in the deformation history when cumulative shear strains were below 5. As deformation continued (cumulative shear strains between 8.57 and 548.57; Table 1) there was a progressive increase in the strength and complexity of the microfabrics developed within the till in response to sinistral (top-to-left) simple shear (KORN 2 to 8; Fig. 11c–i and 17c to i) imposed by the rotating lower platen of the ring shear. The simplest interpretation of the observed fabric geometries is in terms of the progressive development of a set of Riedel shears (Fig. 18) with the individual microfabrics

corresponding to up-shear dipping P-type shears (P-shears), down-shear dipping R-type shears (R-shears), and subhorizontal Y-type shears (Y-shears) (Figs. 13, 14 and 19). Sigmoidal (S-shaped) fabric geometries associated within these Riedel shears (Fig. 18), comparable to S–C and ECC-type fabrics (Passchier and Trouw, 1996; Phillips and Lee, 2011), record a consistent sinistral sense of shear indicating that they all developed in response to the same progressive shear event.

The microfabrics are considered to form by the passive rotation of coarse-silt to sand-grade particles into the plane of the developing fabric(s) (Fig. 20) reflecting the imposed stress field (cf. Hiemstra and Rijsdijk, 2003; Phillips et al., 2011; Phillips et al., 2018a, 2018b). Thomason and Iverson (2006) considered that strong up-glacier ("up-shear") fabrics form in response to the rotation of the till matrix as a result of slip along microshears which will have acted as the bounding surfaces to microscale shear zones leading to the formation of the observed asymmetrical S–C-like fabrics (Figs. 13, 14 and 20). Once aligned parallel to the plane of the developing microfabric, rotation will cease and the clasts will maintain their preferred shape alignment unless there is a change in the orientation of the stress field. Consequently, further deformation and microfabric development will be accommodated by the sliding of grains past one another leading to the lateral propagation of the fabric through the till and the progressive lengthening of the microfabric domains. Sliding of the grains once they are aligned within the fabrics will be facilitated by shear associated within the P, R and Y-type Riedel shears (Fig. 20d, b and c).

In general, the strength and in particular complexity of the microfabrics increases with increased cumulative shear strain (Fig. 17c–i and 19b to i). However, these relationships do not record a simple progression from an earlier formed "S1" microfabric to a later "S2" fabric as described in a number of previous studies (e.g. Phillips et al., 2011; Vaughan-Hirsch et al., 2013; Gehrmann et al., 2017; Narloch et al., 2020). In samples KORN 3, 6 and 7 (Fig. 13a,

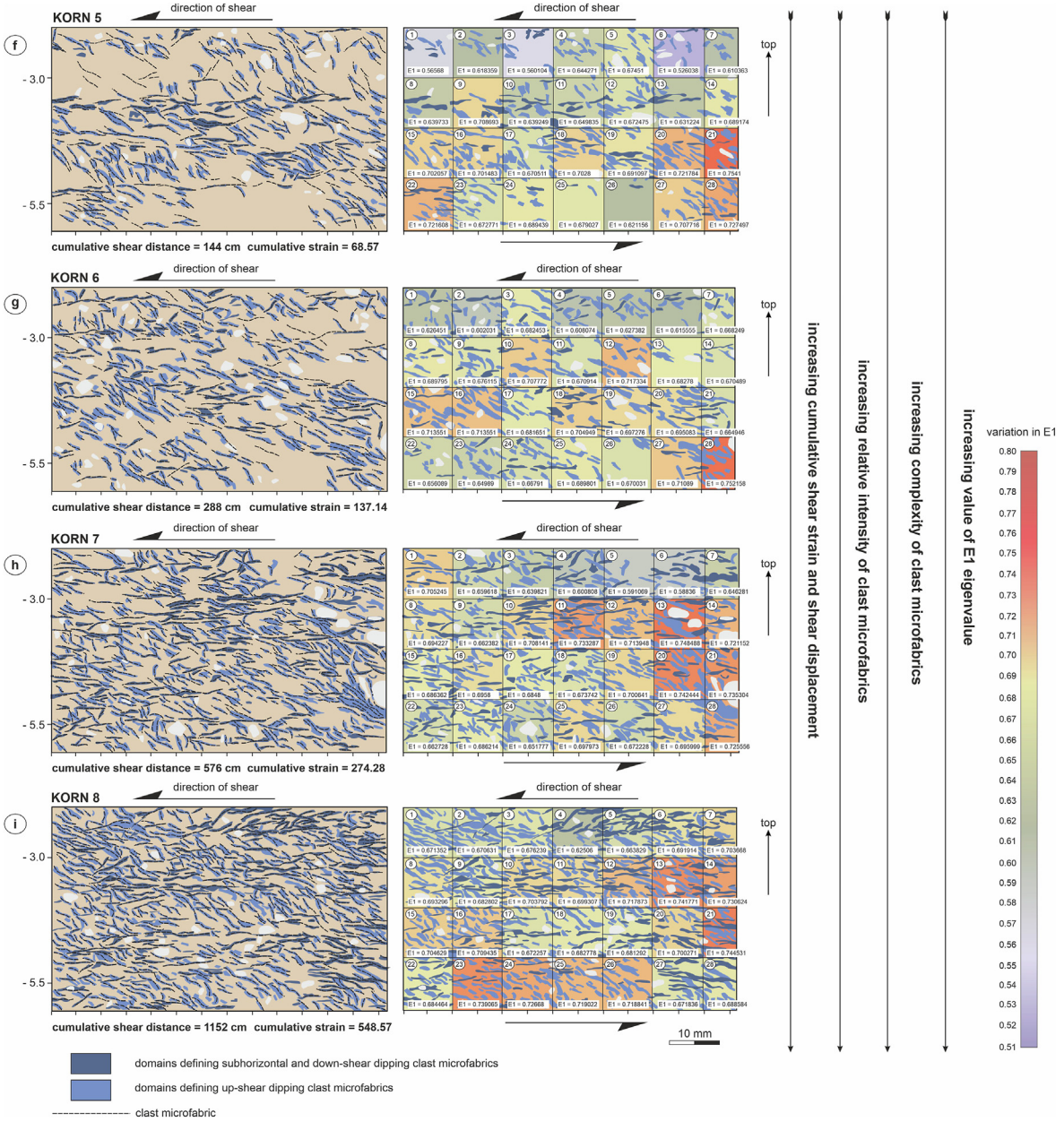

Fig. 17. (*continued*).

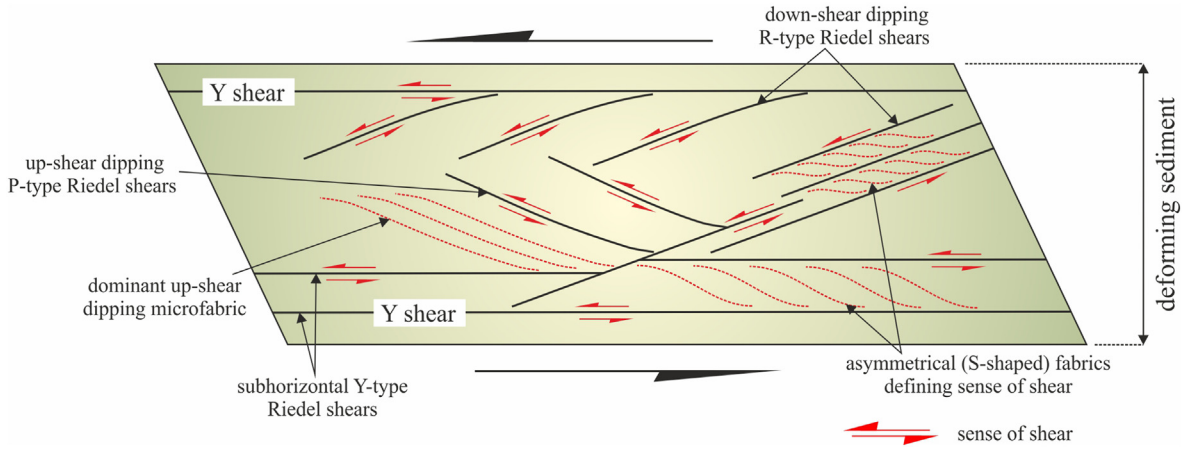

Fig. 18. Diagram showing the relationships between the different sets of Riedel shears developed in response to sinistral simple shear.

c and d, and 17c, g and h) the subhorizontal fabric is crosscut by narrow, moderately dipping (~30°–40°) bands of the up-shear dipping fabric defining narrow P-shears which clearly post-date the formation of the Y-shears (Fig. 19c, d and h). However, in samples KORN 4, 8 and, to a lesser extent, 5 the narrow P-shears and the associated cross-cutting up-shear dipping microfabric are either very weakly developed or absent (Fig. 19e, i, f, respectively). These microstructural relationships clearly demonstrate that microfabric development switched between the imposition of the steeply inclined up-shear dipping fabric (P-shears) to a more widely spaced subhorizontal microfabric (Y-shears). These complex microstructural relationships are consistent with the process of reactivation and re-use of the earlier formed fabrics during subsequent stages of the progressive simple shear deformation imposed by the ring shear. This complexity has been recognised within deformed rocks for some time, especially within shear zones which can record a prolonged history of deformation/movement where the progressive shearing operates in a synthetic sense along pre-existing foliations in subsequent events leading to the development of a composite foliation (e.g. Bell, 1985, 1986; Davis and Forde, 1994; Passchier and Trouw, 1996; Nyman, 1999; Williams et al., 2001). The renewed development of pre-existing fabrics can therefore lead to difficulties in determining temporal and spatial relationships of these fabrics to larger structures as well as their correlation to individual tectonic events (i.e. D1, D2, Dn … etc).

The resulting model of microfabric development in the Kórnik till in response to progressive simple shear is shown in Fig. 19. The orientation of the up-shear dipping fabric (P-shears) with respect to the imposed sinistral simple shear means that this fabric would have been under compression. In contrast, the R-shears, defined by the down-shear dipping fabric, are extensional structures with the subhorizontal fabric (Y-shears) occurring coplanar to the margins of the shear zone. The observed complex microfabric relationships described above are interpreted as recording deformation partitioning within the till at a microscale, leading to the switching from localised imposition of the up-shear dipping compressional fabric and P-shear formation, to subhorizontal shear and down-shear dipping fabric development leading to Y-shear formation accompanied by extension and the growth of low-angle R-shears, and back again (Fig. 19).

The proposed switching between the imposition of compressional and subhorizontal shear related fabrics may potentially reflect the fluctuations of the shear stress curve shown on Fig. 12; this figure also shows the points at which samples KORN 0 to 8 were collected. Below a shear length of 600 cm fluctuations in the curve define a number of broad cycles which show a pattern of increasing shear stress followed by a steep fall. At shear distances of ≥600 cm these fluctuations are more pronounced/closely spaced (wavelength of 45–50 cm) leading to a marked oscillation of the stress curve (Fig. 12a). Importantly, these fluctuations correspond to the progressive development of shear related fabrics in the Kórnik till (KORN 5 to 8; Fig. 12f–i and 19f to i). Compression leading to the imposition of the up-shear dipping microfabric defining the P-shears will have led to an increase in both sediment packing and density/number of intergranular contacts, leading to a progressive increase in shear stress (Fig. 12b). In contrast, subsequent movement along the developing Y-shears and extension on the down-shear dipping R-shears would have led to a release of this stress and marked fall in shear stress curve (Fig. 12b). The magnitude of this fall may reflect the amount or duration of the displacement (slip) along the Y- and R-shear surfaces. If this interpretation is correct, then the fluctuations in the shear stress curve between KORN 7 and 8 (Fig. 12a) may correspond to phases of movement along the well-developed subhorizontal shears within these samples (Figs. 14 and 19h, i). Consequently, the proposed model of deformation and fabric development within the Kornik till during the ring shear experiment is one involving alternating phases of "stick" (compression = P-shear development) and "slip" (subhorizontal shear = Y- and R-shear development).

6. Implications for soft-sediment deformation beneath glaciers and ice sheets

6.1. Modelling of microfabric development within naturally occurring subglacial traction tills

Detailed microscale analysis of the microfabrics developed during the ring shear experiment are directly comparable to the fabrics observed within the naturally deformed till within the bed of the OPIS; in particular the formation of a complex array of simulated up-ice and down-ice dipping Riedel shears and a subhorizontal shear fabric (compare thin section KORN 8 (this study) shown in Fig. 14 with sample C1 (Phillips et al., 2018a, 2018b) in Fig. 21) (Spagnolo et al., 2016; Phillips et al., 2018b). Phillips et al. (2018b) concluded that the cross-cutting relationships between the microfabrics record temporal changes in the style and relative age of deformation in the bed of the OPIS, becoming progressively younger upwards, compatible with shear having accompanied incremental till accretion at the top of the bed (see Fig. 17 of Phillips et al., 2018b), and the time-transgressive accretion and

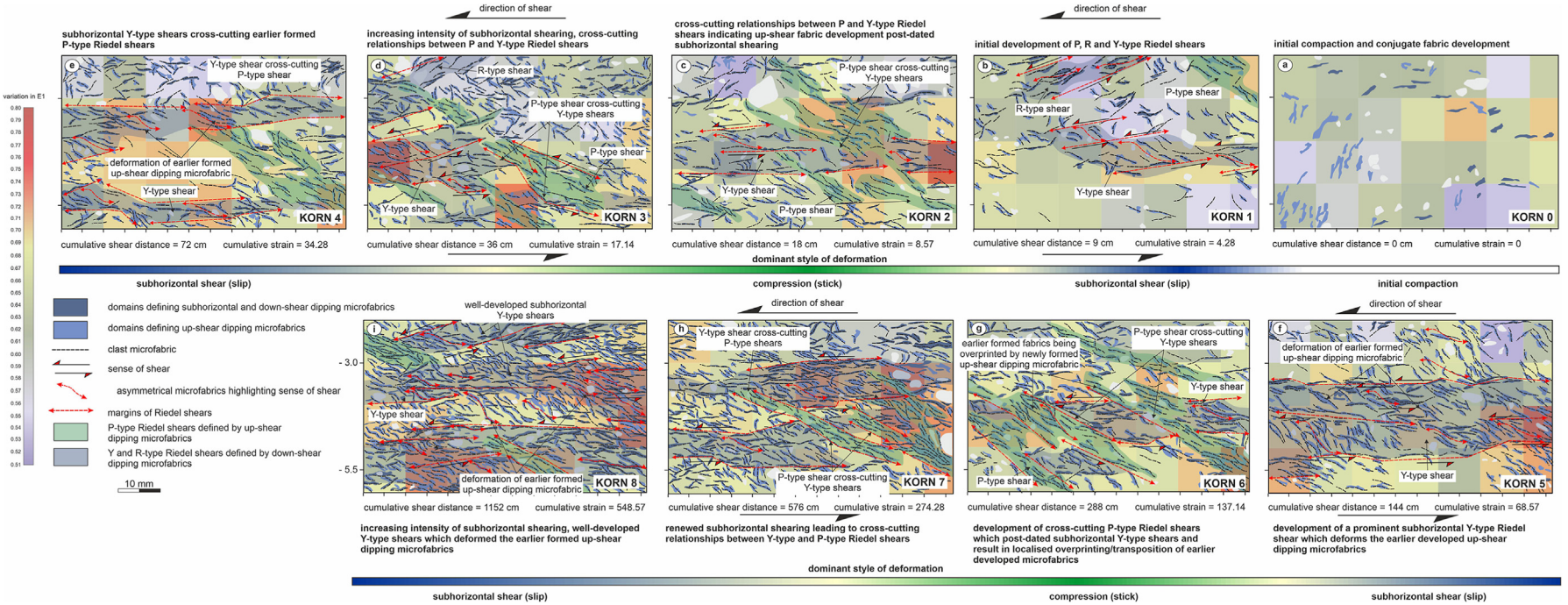

Fig. 19. Diagram showing the proposed conceptual model of microfabric development in response to progressive simple shear deformation (see text for details): **(a)** KORN 0; **(b)** KORN 1; **(c)** KORN 2; **(d)** KORN 3; **(e)** KORN 4; **(f)** KORN 5; **(g)** KORN 6; **(h)** KORN 7; and **(i)** KORN 8.

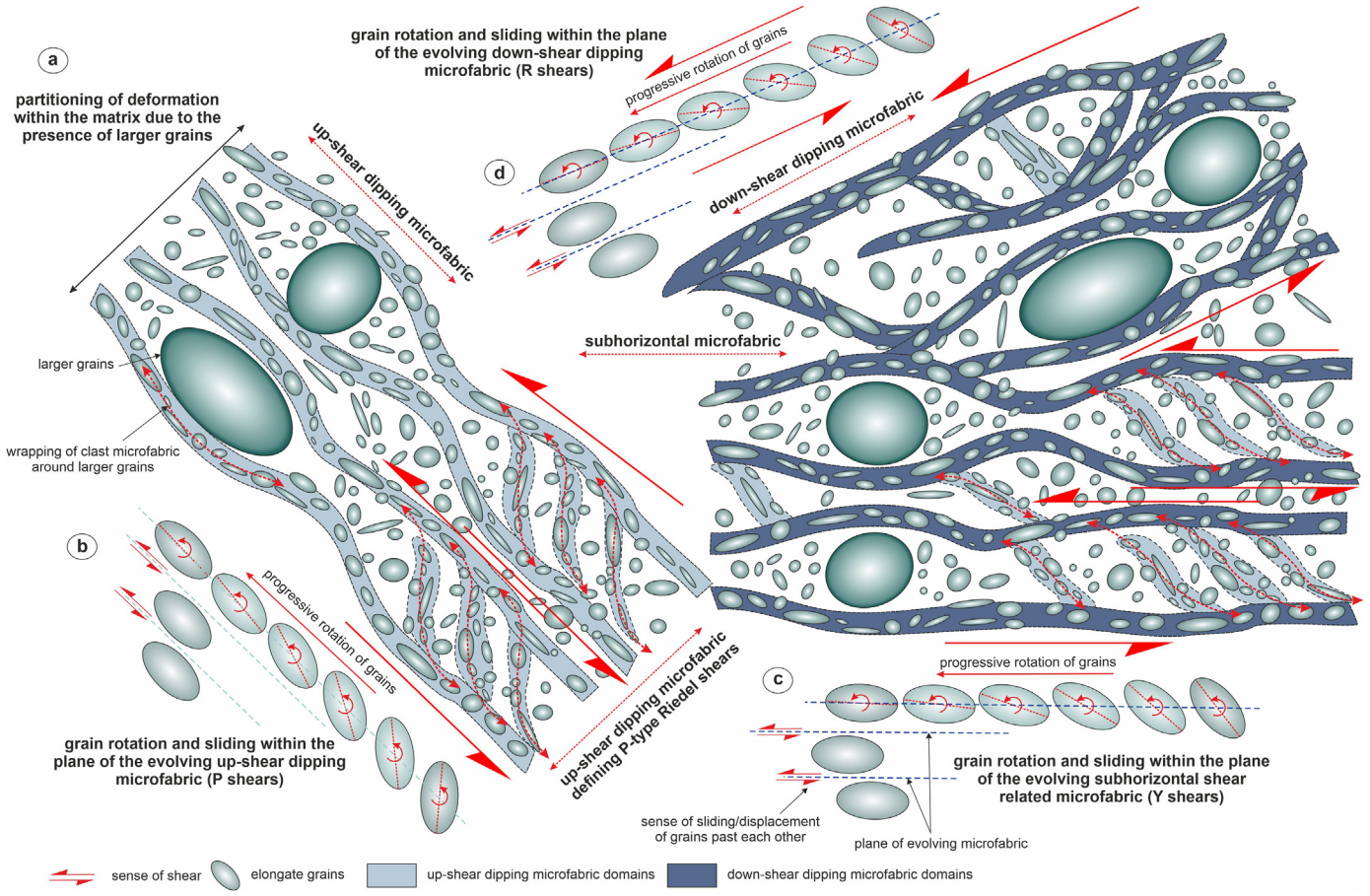

Fig. 20. (a) Diagram showing the development of anastomosing up-shear (P-type Riedel shears), down-shear (R-type Riedel shears) and subhorizontal microfabrics (Y-type Riedel shears) within a till defined by the preferred shape alignment of finer grained clasts. Deformation partitioning within the till and the spacing of the microfabric domains is locally controlled by the grain size and spacing of the larger sand to pebble sized clasts; **(b)**, **(c)** and **(d)** cartoons showing the passive rotation of elongate clasts into the plane of the developing microfabrics. Further deformation of clasts aligned within this fabric is thought to occur in response to grain sliding.

deformation model of till by Larsen et al. (2004). In addition, these authors suggested that the variation in microfabric strength within the Kórnik till recorded changes in the magnitude of the cumulative strain and the degree of coupling between the OPIS and its bed. Microstructural relationships preserved within the Kórnik till led Phillips et al. (2018b) to conclude that the earlier stages of ductile shearing within the bed of the OPIS were dominated by the imposition of a subhorizontal shear (Y-shears) fabric (S2 of Phillips et al., 2018b). This earlier formed microfabric was superseded by the development of an up-ice dipping fabric (S3) and finally a down-ice dipping fabric (S4) defining cross-cutting P- and R-type shears, respectively. However, detailed analysis of the microfabrics formed during the ring shear experiment (this study) clearly indicates that microfabric development can switch between the imposition of an up-shear and down-shear dipping fabrics (Fig. 19), and back again, leading to the potential preservation of a complex array of cross-cutting relationships between these microfabrics. Consequently, microfabric relationships observed in the Kórnik and other naturally occurring subglacial traction tills are likely to record the dominant style of deformation which was active when shear imposed by the overriding ice ceased, either due to continued till accretion at the top of the bed or the cessation of forward movement of the ice.

Although the ring shear experiment carried out during this study clearly replicated shear related microfabric development within the bed of the OPIS, it did not replicate the microstructures formed in response to later (post-shear) process. Phillips et al. (2018b) identified an anastomosing, subvertical microfabric which crosscut all the earlier shear-related fabrics within the till (see Fig. 15 of Phillips et al., 2018b) which the authors interpreted as having formed in response to increased dewatering with depth as a function of the increased vertical load. Studies of tills from the beds of contemporary (Alley et al., 1986; Tulaczyk et al., 1998) and palaeo- (Ó Cofaigh et al., 2007) ice streams indicate that they are typically highly porous and weak, with a water content close to the liquid limit. Microfabric development associated with the initial consolidation (prior to shearing) of sample KORN 0 (Fig. 11) clearly indicates that water-rich tills are highly responsive to any applied stress even at very low cumulative strains (see Fig. 15). The OPIS is likely to have been several hundred metres thick and therefore would have exerted a significant vertical load on its bed leading to compaction and dewatering of the till shortly after its deposition. The degree of compaction of the bed of the OPIS is likely to have continued after subglacial shearing associated with fast ice flow had ceased, leading to continued dewatering of the till decreasing its porosity and permeability. These results also have implications for other micromorphological studies, which tend to interpret all of the microstructures in terms of subglacial shearing. The clear evidence provided by this study demonstrates that water-saturated tills are high responsive to any applied stress field (c.f. Thomason and Iverson, 2006). This means that the potential impacts of loading by static ice and/or reworking of the till by secondary mass

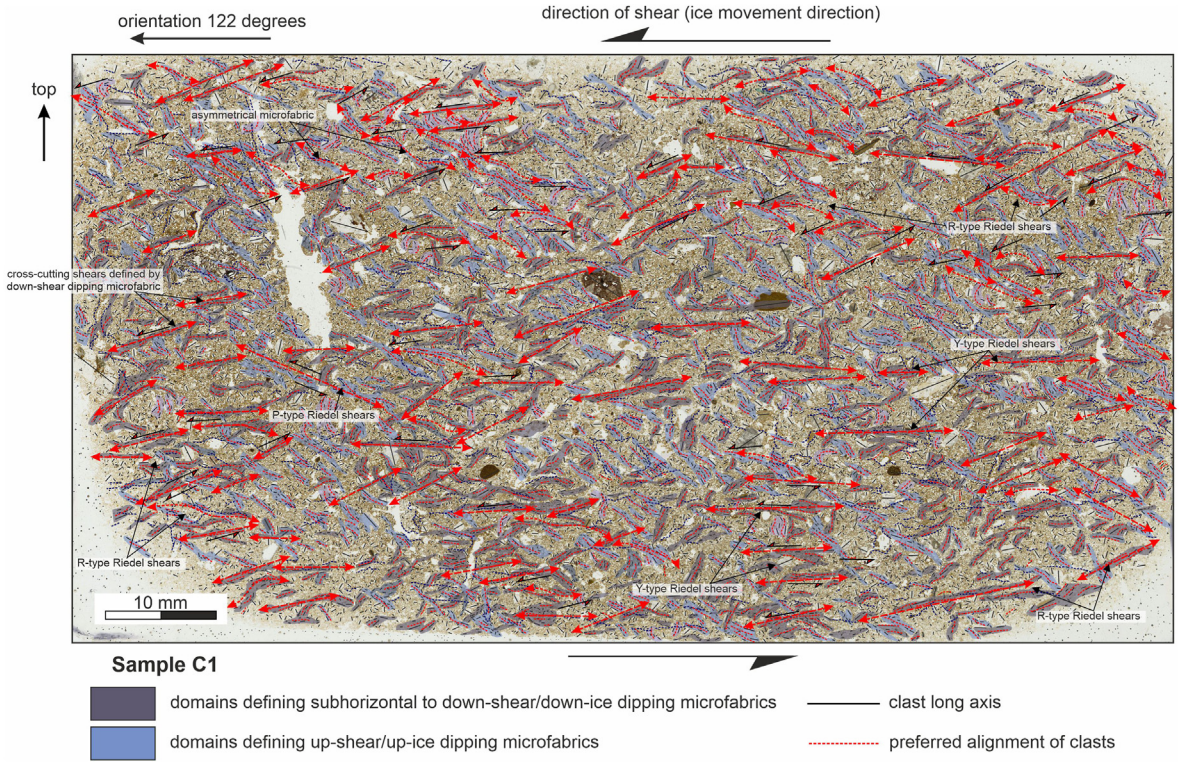

Fig. 21. Structural interpretation of the microfabrics developed within the Kórnik till (sample C1 of Phillips et al., 2018b) showing the complex fabric relationships associated with the development of subhorizontal Y-type shears, down-shear dipping R-type shears and up-shear dipping P-type Reidel shears (see text for details).

movement and periglacial processes once the till is revealed by the retreating ice needs to be carefully taken into consideration.

6.2. Potential stick-slip style of ice movement due to changes in the style of bed deformation?

Stick-slip forward motion of a glacier or ice sheet is widely considered to reflect fluctuations in water pressures at the ice-bed interface leading to repeated coupling (stick) and bed deformation, followed by decoupling (slip) preventing the transmission of stress into the underlying till (Fischer and Clarke, 1997). The degree of coupling can also be controlled by the granularity of the sediments with low permeability clay-rich tills promoting decoupling and basal sliding (Piotrowski and Tulaczyk, 1999; Piotrowski et al., 2006), and more free-draining sandy tills leading to increased coupling and bed deformation (Boulton, 1986; Engelhardt and Kamb, 1998). However, results of this study suggest that a stick-slip style of movement may potentially also be occurring during bed deformation in response to changes in the dominant style of deformation being accommodated by the till. During the ring shear experiment, microfabric development switched between the imposition of the steeply inclined up-shear dipping P-shear related fabric, to a more widely spaced subhorizontal fabric defining the Y-shears, and back again (Fig. 19). The orientation of the P, R and Y shears with respect to the sinistral simple shear being imposed on the till by the ring shear means that they are either under compression (P-shears), extension (R-shears) or occur coplanar to the imposed shear (Y-shears). Compression will lead to an increase in the packing of the sediment and contacts between the constituent grains, leading to the observed increase in shear stress (Fig. 12). In effect this will "stiffen" the till leading to a greater degree of coupling of the ice to the bed. In contrast, movement along the subhorizontal Y-shears and extension on the down-shear dipping R-shears will release this stress (Fig. 12) and potentially failure leading to slip along these surfaces. Slip along the subhorizontal (Y-shear) microfabric may result in the commonly observed fissility (and associated slickensides) in subglacial traction tills (see Fig. 10.14 in Evans, 2018). The overall model of bed deformation established from the ring shear experiment is therefore one of alternating phases of "stick" (compression = P-shear development) and "slip" (subhorizontal shear = Y- and R-shear development) (Fig. 19). The magnitude of these bed deformation related stick-slip events is likely to be relatively small in comparison to the switching between basal sliding and bed deformation outlined above. In addition, due to the heterogeneous nature of microfabric development on a macro and microscale they are likely to be very localised within the bed.

6.3. Deformation paths and estimating cumulative strains during subglacial deformation

Phillips et al. (2018b) used the variation in E1 eigenvalues to quantify the variation in the relative microfabric strength within the Kórnik till demonstrating that fabric strength not only varies on a microscale, but also vertically upwards through the till sequence towards the base of the OPIS (see Figs. 13 and 14a of Phillips et al., 2018b). Although consistent with the increased displacement towards the base of the overriding ice proposed by Boulton and Hindmarsh (1987) in support of the deforming bed model, the low fabric strengths encountered in the lower part of the bed of the OPIS may simply reflect the degree of overprinting during the later dewatering of the till. In addition, Phillips et al. (2018a, 2018b) projected the E1 eigenvalues calculated for the Kórnik till onto the shear strain curve for the sand-rich Douglas till of Thomason and Iverson (2006) (see Fig. 14b of Phillips et al., 2018a, 2018b), concluding that *if* this approach was valid then the amount of shear

being transmitted into the bed of the OPIS was low with potential strains of <15. However, in the absence of any reliable strain markers (e.g. deformed clasts known to have been originally circular in shape) estimating the magnitude of the shear strains imparted on tills by the overriding ice remains problematic. Several published studies have used the relative abundance of selected microstructures (e.g. microshears, grain stacks) as proxies for estimating strain in subglacial traction tills (Larsen et al., 2006, 2007; Narloch et al., 2012). However, not only is the identification of such microstructures qualitative and potentially subjective

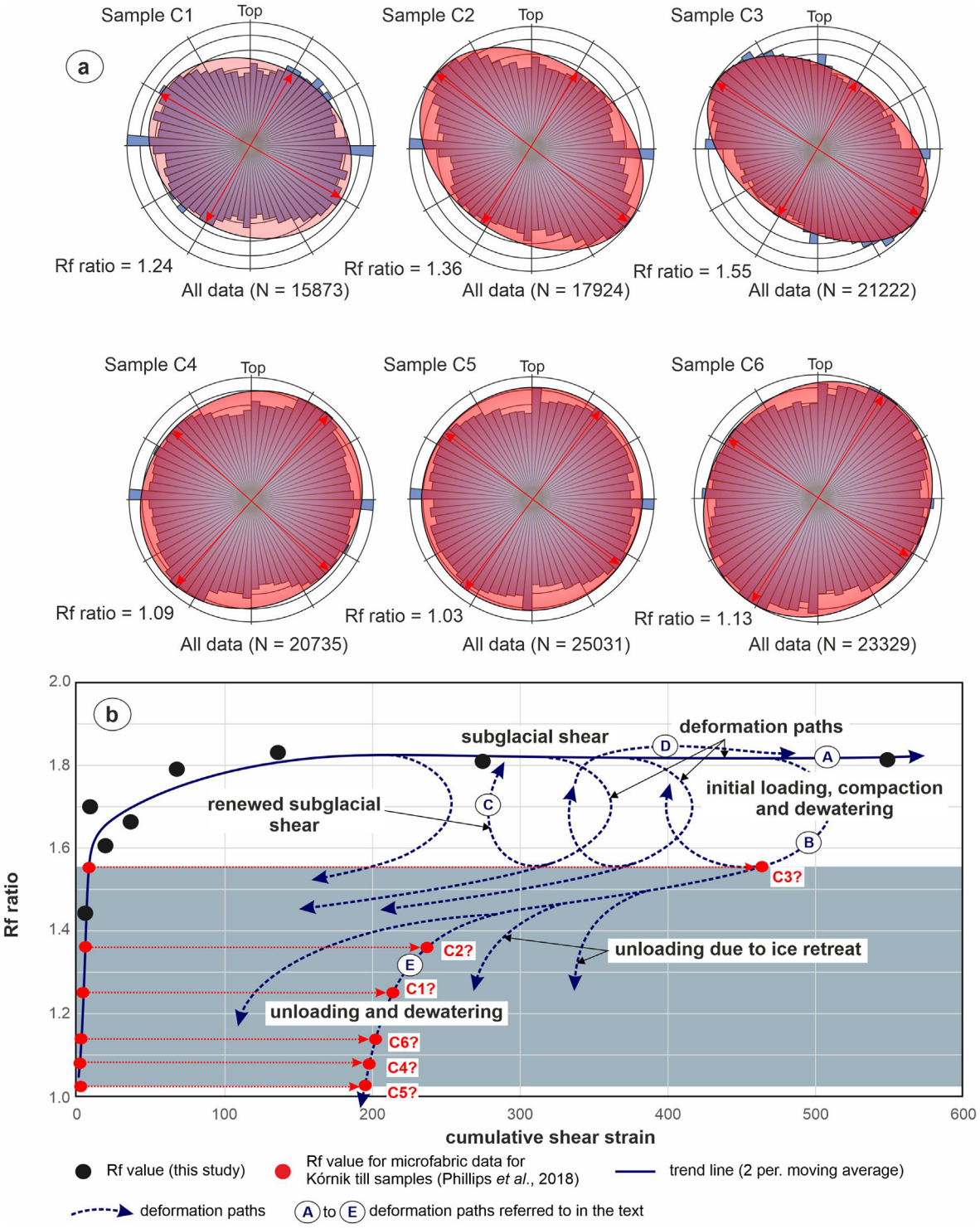

Fig. 22. (a) Rose diagrams showing variation in clast long axis orientation in samples C1 to C6 of Phillips et al. (2018b) and the calculated Rf ratio (Rf = long axis/short axis) of the ellipse enclosing these data; and **(b)** plot of Rf ratio versus cumulative strain for the till deformed during the ring shear experiments and the Kornik till (samples C1 to C6; Phillips et al., 2018b). Also shown are the potential deformation paths followed by subglacial traction tills in response to repeated cycles of subglacial shearing, loading and dewatering (see text for details).

(Leighton et al., 2012; Neudorf et al., 2013), their development can be strongly lithologically controlled, e.g. microshears defined by a unistrial plasmic fabrics will only form in clay-rich sediments.

Very low strain values for the Kórnik subglacial traction till are also indicated by plotting the calculated E1 eigenvalues and Rf values (below 20) for this till on the cumulative strain curves established during the present study (Fig. 22b). This is possible if forward motion of the OPIS was largely accommodated by basal sliding rather than bed deformation and the ice was effectively decoupled from its bed. However, visually, the relative strength of the microfabrics observed in the Kórnik till (samples C1, C2 and C3 of Phillips et al., 2018a, 2018b) are comparable to those within KORN 8 (compare Figs. 14 and 21) indicating that the cumulative strains encountered beneath the OPIS were far higher than predicted by simply plotting the E1 eigenvalues and/or Rf ratio onto the experimentally defined cumulative strain curve. The present study indicates that water-rich sediments can be highly responsive to shear stress even at very low strains. Consequently, one explanation for the discrepancy in estimated cumulative strains for naturally deformed tills (e.g. the Kórnik till) using experimentally determined cumulative strain curves could be due to subsequent (post-shear) processes leading to a reduction in fabric strength and the partial or complete overprinting of earlier formed shear related structures (Section 6.1).

Although microfabric development in naturally occurring subglacial traction tills can be investigated using ring shear experiments, the deformation histories recorded by these tills will be far more complex. Naturally occurring tills will have undergone repeated cycles of subglacial shear, dewatering and/or dilation due to changes in porewater content and/or pressure, periods of loading and unloading and compaction when the overlying ice stops moving, etc. As a result natural subglacial traction tills will follow a more complex "deformation path" (cf. Menzies, 2012; Menzies et al., in press) than the simple strain curve followed by the experimentally deformed till (Fig. 22b). Initial microfabric development within tills in response to progressive subglacial shearing is likely to closely follow the cumulative strain curve defined by the KORN samples with an initial rapid increase in fabric strength (i.e. Rf ratio) at low cumulative strains, flowed by a more gradual increase in fabric strength at high cumulative strains (Path A on Fig. 22b). However, when forward motion of the ice pauses (e.g. during a period of quiescence after a surge event) or stops, loading of the water-rich till by the overlying static ice will lead to initial compaction and dewatering of the till potentially accompanied by the modification or even overprinting (loss) of earlier formed shear fabrics. The resulting deformation path followed by the till is likely to show a reduction in Rf ratio and, to a lesser extent, cumulative strain (Path B on Fig. 22b).

Renewed movement of the ice and transmission of shear into the bed will reinitiate microfabric development with the deformation path followed by the till showing an increase in Rf ratio (i.e. fabric strength) and cumulative strain rate (Path C on Fig. 22b). After an initial rapid increase in fabric strength the evolving deformation path is likely to follow a similar path to the ring shear experiment: increasing cumulative strain with only a minor gradual increase in relative fabric strength (Rf ratio) (Path D on Fig. 22b). Unless there is a change in the orientation of the stress field, renewed bed deformation will simply lead to the reactivation of the pre-existing microfabrics with the till. Due to the heterogenous nature of bed deformation the reactivation of the existing fabrics will result in a complex array of cross-cutting relationships between these fabrics. Consequently, it may be difficult to establish the relative ages of the microfabrics (S1, S2, S3, etc.) and the number of phases of deformation (D1, D2, D3, etc.) encountered by the till. Repeated movement of the glacier will lead to a more complex deformation path comprising several "cycles" of microfabric development of differing magnitudes, potentially separated by periods of "fabric loss" due to the overprinting of the shear-related fabrics associated with reorganisation of the sediment packing during compaction and dewatering.

Deglaciation and exposure of the bed will result in dewatering of the till and potential in situ reworking by periglacial processes (freeze thaw) are likely to lead in a rapid fall of Rf ratio as the earlier formed shear related fabrics are variably overprinted (Path E on Fig. 22b). In addition, water-rich tills exposed at the ice margin may undergo mass-flow leading to the complete loss of the earlier subglacial strain signature and the development of a comparable set of flow-related structures (Phillips et al., 2022). The cumulative strain signature will not be zeroed as the tills are likely to preserve at least some imprint of the earlier subglacial deformation. Overprinting of earlier fabrics due to dewatering and other post-shear processes is thought to result in the low fabric strengths (Rf values) observed within the Kórnik tills (see Fig. 22a). The Rf values calculated for samples C1 to C6 have been projected onto deformation path E shown on Fig. 22b to illustrate how post-shear modification of the Kórnik till may have impacted the estimates of cumulative strains.

7. Conclusions

The detailed micromorphological study of microfabric development in nine thin sections of experimentally deformed till subject to simple shear in a ring shear apparatus has been used to investigate the progressive development of a range of microfabrics during soft-sediment deformation. The study clearly reveals that microfabric development is heterogeneous, reflecting the partitioning of deformation at a microscale and that the relative strength and complexity of the microfabrics increases with increasing cumulative shear distance and strain (KORN 0 - cumulative shear distance = 0 cm, cumulative strain = 0; to KORN 8 - cumulative shear distance = 1152 cm, cumulative strain = 549). A conjugate microfabric formed during the initial consolidation and draining of the till (prior to shear) highlighting that unconsolidated water-rich sediments are highly responsive to any applied stress, even at very low strains. This fabric was subsequently overprinted at a very early stage of the ring shear experiment (cumulative strain <5) with continued deformation leading to the progressive development of a range of microfabrics defining up-shear dipping P-shears, down-shear dipping R-shears, and subhorizontal Y-shears. Comparable fabrics have been described in published studies of the Kórnik till which forms the bed of the Odra Palaeo-Ice Stream in western Poland indicating that ring shear experiments can be used to investigate the deformation occurring beneath glaciers and ice sheets. Changes in the relationships between the microfabrics record the switching between localised (microscale) compression and P-shear formation, to subhorizontal shear and the formation of Y-shears accompanied by extension and the growth of low-angle R-shears, and back again. This process may potentially lead to alternating phases of "stick" (compression) and "slip" (subhorizontal shear) recognised as a key feature of glacier motion occurring in response to soft-sediment bed deformation.

Credit author statement

Emrys Phillips – Micromorphological analysis, writing of paper (lead author), drafting of figures, major contribution to developing scientific ideas within the paper. Jan Piotrowski – Ring shear experiments, writing of paper (co-author), major contribution to developing scientific ideas within the paper

Declaration of competing interest

The authors declare that they have no known competing financial interests or personal relationships that could have appeared to influence the work reported in this paper.

Data availability

Data will be made available on request.

Acknowledgements

We thank Mia Bering Holdensen for help with the ring-shear experiments and Adrian Palmer for thin-section production. The ring-shear experiments were conducted as part of the Danish Council for Independent Research (FNU) grant DFF-7014-00156 to Jan A. Piotrowski. Jonathan Lee is thanked for his constructive review of an earlier version of this manuscript. John Menzies and Neal Iverson are both thanked for their careful reviews of an earlier version of this paper. Emrys Phillips publishes with the permission of the Executive Director of the British Geological Survey.

References

Alley, R.B., Blankenship, D.D., Bentley, C.R., Rooney, S.T., 1986. Deformation of till beneath ice stream B, West Antarctica. Nature 322, 57–59.
Baroni, C., Fasano, F., 2006. Micromorphological evidence of warm-based glacier deposition from the ricker hills tillite (victoria land, Antarctica). Quat. Sci. Rev. 25, 976–992.
Bateman, M.D., Swift, D.A., Piotrowski, J.A., Sanderson, D.C.W., 2012. Investigating the effects of glacial shearing of sediment on luminescence. Quat. Geochronol. 10, 230–236.
Bateman, M.D., Swift, D.A., Piotrowski, J.A., Rhodes, E.J., Damsgaard, A., 2018. Can glacial shearing of sediment reset the signal used for luminescence dating? Geomorphology 306, 90–101.
Bell, T.H., 1985. Deformation partitioning and porphyroblast rotation in metamorphic rocks: a radical reinterpretation. J. Metamorph. Geol. 3, 109–118.
Bell, T.H., 1986. Foliation development and refraction in metamorphic rocks: reactivation of earlier foliations and decrenulation due to shifting patterns of deformation partitioning. J. Metamorph. Geol. 4, 421–444.
Bering Holdensen, M., 2017. Laboratory Experiments on Sediment Deformation by Ice Sheets. M.Sc. Thesis. Aarhus University, p. 148.
Blankenship, D.D., Bentley, C.R., Rooney, S.T., Alley, R.B., 1986. Seismic measurements reveal a saturated porous layer beneath an active Antarctic ice stream. Nature 322, 54–57.
Boulton, G.S., 1986. A paradigm shift in glaciology? Nature 322, 18.
Boulton, G.S., Hindmarsh, R.C.A., 1987. Sediment deformation beneath glaciers: rheology and geological consequences. J. Geophys. Res. 92, 9059–9082.
Brumme, J., 2015. Three-dimensional Microfabric Analyses of Pleistocene Tills from the Cliff Section Dwasieden on Rügen (Baltic Sea Coast): Micromorphological Evidence for Subglacial Polyphase Deformation (PhD Thesis). Ernst-Moritz-Arndt-Universitstäat, Greifswald, p. 210.
Carr, S.J., Goddard, M.A., 2007. Role of particle size in till-fabric characteristics: systematic variation in till fabric from Vestari-Hagafellsjökull, Iceland. Boreas 36, 371–385.
Carr, S.J., Haflidason, H., Sejrup, H.P., 2000. Micromorphological evidence supporting late Weichselian glaciation of the northern North Sea. Boreas 29, 315–328.
Damsgaard, A., Egholm, D., Piotrowski, J.A., Tulaczyk, S., Larsen, N.K., Tylmann, K., 2013. Discrete element modelling of subglacial sediment deformation. J. Geophys. Res. – Earth Surface 118, 1–13.
Damsgaard, A., Egholm, D.L., Piotrowski, J.A., Tulaczyk, S., Larsen, N.K., Brædstrup, C.F., 2015. A new methodology to simulate subglacial deformation of water-saturated granular material. Cryosphere 9, 2183–2200.
Davis, B.K., Forde, A., 1994. Regional slaty cleavage formation and fold axis rotation by re-use and reactivation of pre-existing foliations: the Fiery Creek Slate Belt, North Queensland. Tectonophysics 230, 161–179.
Dreimanis, A., 1988. Tills: their genetic terminology and classification. In: Goldthwait, R.P., Matsch, C.L. (Eds.), Genetic Classification of Glacigenic Deposits. Balkema, Rotterdam, pp. 17–84.
Engelhardt, H., Kamb, B., 1998. Basal hydraulic system of a West Antarctic ice stream: constraints from borehole observations. J. Glaciol. 43, 207–230.
Evans, D.J.A., 2018. Till. A Glacial Process Sedimentology. J. Wiley & Sons Ltd., UK, p. 390.
Evans, D.J., Phillips, E.R., Hiemstra, J.F., Auton, C.A., 2006. Subglacial till: formation, sedimentary characteristics and classification. Earth Sci. Rev. 78, 115–176.
Fischer, U., Clarke, G.K.C., 1997. Stick-slip sliding behaviour at the base of a glacier. Ann. Glaciol. 24, 390–396.
Gehrmann, A., Hüneke, H., Meschede, M., Phillips, E., 2017. 3D microstructural architecture of deformed glacigenic sediments associated with large-scale glacitectonism, Jasmund Peninsula (NE Rügen), Germany. J. Quat. Sci. 32, 213–230. https://doi.org/10.1002/jqs.2843.
Head, K.H., 1989. Soil Technician's Handbook. John Wiley and Sons, New York, p. 83.
Hiemstra, J.F., van der Meer, J.J.M., 1997. Pore-water controlled grain fracturing as an indicator for subglacial shearing in tills. J. Glaciol. 43, 446–454.
Hiemstra, J.F., Rijsdijk, K.F., 2003. Observing artificially induced strain: implications for subglacial deformation. J. Quat. Sci. 18, 373–383.
Hogan, K.A., Arnold, N.S., Larter, R.D., Kirkham, J.D., Noormets, R., Ó Cofaigh, C., Golledge, N.R., Dowdeswell, J.A., 2022. Subglacial water flow over an Antarctic palaeo-ice stream bed. J. Geophys. Res.: Earth Surf. 127. https://doi.org/10.1029/2021JF006442.
Hooke, R.L., Iverson, N.R., 1995. Grain-size distribution in deforming subglacial tills: role of grain fracture. Geology 23, 57–60.
Hooyer, T.S., Iverson, N.R., 2000. Clast-fabric development in a shearing granular material: implications for subglacial till and fault gouge. Geol. Soc. Am. Bull. 112, 683–692.
Hooyer, T.S., Iverson, N.R., Lagroix, F., Thomason, J.F., 2008. Magnetic fabric of sheared till: a strain indicator for evaluating the bed deformation model of glacier flow. J. Geophys.l Res.-Earth Surf. 113, F02002.
Iverson, N.R., 2010. Shear resistance and continuity of subglacial till: hydrology rules. J. Glaciol. 56, 1104–1114.
Iverson, N.R., Zoet, L.K., 2015. Experiments on the dynamics and sedimentary products of glacier slip. Geomorphology 244, 121–134.
Iverson, N.R., Hooyer, T.S., Hooke, R.L., 1996. A laboratory study of sediment deformation: stress heterogeneity and grain-size evolution. Ann. Glaciol. 22, 167–175.
Iverson, N.R., Hooyer, T.S., Thomason, J.F., Graesch, M., Shumway, J.R., 2008. The Experimental Basis for Interpreting Particle and Magnetic Fabrics of Sheared till, vol. 33, pp. 627–664.
Iverson, N.R., Baker, R.B., Hooyer, T.S., 1997. A ring shear device for the study of till deformation: tests on tills with contrasting clay content. Quat. Sci. Rev. 16, 1057–1066. https://doi.org/10.1016/S0277-3791(97)00036-X.
Iverson, N.R., Hooyer, T.S., Baker, R.W., 1998. Ring-shear studies of till deformation: coulomb-plastic behaviour and distributed strain in glacier beds. J. Glaciol. 44, 634–642.
Jørgensen, F., Piotrowski, J.A., 2003. Signature of the baltic ice stream on Funen island, Denmark during the weichselian glaciation. Boreas 32, 242–256.
Khatwa, A., Tulaczyk, S., 2001. Microstructural interpretations of modern and Pleistocene subglacially deformed sediments: the relative role of parent material and subglacial processes. J. Quat. Sci. 16, 507–517.
Larsen, N.K., Piotrowski, J.A., Kronborg, C., 2004. A multiproxy study of a basal till: a time-transgressive accretion and deformation hypothesis. J. Quat. Sci. 19, 9–21.
Larsen, N.K., Piotrowski, J.A., Christiansen, F., 2006. Microstructures and microshears as proxy for strain in subglacial diamicts: implications for basal till formation. Geology 34, 889–892.
Larsen, N.K., Piotrowski, J.A., Menzies, J., 2007. Microstructural evidence of low-strain, time transgressive subglacial deformation. J. Quat. Sci. 22, 593–608.
Leighton, I.D., Hiemstra, J.F., Weidman, C.T., 2012. Recognition of micro-scale deformation structures in glacial sediments – pattern perception, observer bias and the influence of experience. Boreas 42, 463–469. https://doi.org/10.1111/j.1502-3885.2011.00246.x.
van der Meer, J.J.M., Menzies, J., 2011. The micromorphology of unconsolidated sediments. Sediment. Geol. 238, 213–232.
van der Meer, J.J.M., Menzies, J., Rose, J., 2003. Subglacial till, the deformable glacier bed. Quat. Sci. Rev. 22, 1659–1685.
van der Meer, J.J.M., Kjær, K.H., Krüger, J., Rabassa, J., Kilfeather, A.A., 2009. Under pressure: clastic dykes in glacial settings. Quat. Sci. Rev. 28, 708–720.
Menzies, J., 2002. Modern and Past Glacial Environments. Butterworth-Heinemann Ltd., p. 543
Menzies, J., 2000. Micromorphological analyses of microfabrics and microstructures indicative of deformation processes in glacial sediments. In: Maltman, A.J., Hubbard, B., Hambrey, M.J. (Eds.), Deformation of Glacial Materials, vol. 176. Geological Society of London, Special Publication, pp. 245–257.
Menzies, J., 2012. Strain pathways, till internal architecture and microstructures – perspectives on a general kinematic model – a 'blueprint' for till development. Quat. Sci. Rev. 50, 105–124.
Menzies, J., van der Meer, J.J.M., Rose, J., 2006. Till – a glacial "tectomict", a microscopic examination of a till's internal architecture. Geomorphology 75, 172–200.
Menzies, J., Paulen, R.C., Rice, J.M. . Time-transgressive evolution of microstructures in subglacial tills. Sedimentology..
Moore, P.L., Iverson, N.R., 2002. Slow episodic shear of granular materials regulated by dilatant strengthening. Geology 30, 843–846.
Narloch, W., Piotrowski, J.A., Wysota, W., Larsen, N.K., Menzies, J., 2012. The signature of strain magnitude in tills associated with the Vistula Ice Stream of the Scandinavian Ice Sheet, central Poland. Quat. Sci. Rev. 57, 105–120.
Narloch, W., Piotrowski, J.A., Wysota, W., Tylmann, K., 2015. Till formation under a soft-bedded palaeo-ice stream of the Scandinavian Ice Sheet, constrained using qualitative and quantitative microstructural analyses. Sediment. Geol. 326, 64–78.
Narloch, W., Phillips, E.R., Piotrowski, J.A., Ćwiek, M., 2020. Patterns of deformation within a subglacial shear zone: implications for palaeo-ice stream bed evolution. Sediment. Geol. 397. https://doi.org/10.1016/j.sedgeo.2019.105569.

Neudorf, C.M., Brennand, T.A., Lian, O.B., 2013. Till-forming processes beneath parts of the Cordilleran Ice Sheet, British Columbia, Canada: macroscale and microscale evidence and a new statistical technique for analysing microstructure data. Boreas. https://doi.org/10.1111/bor.12009.ISSN0300-9483.
Nyman, M.W., 1999. Fabric reactivation: an example from the hualapai mountains, NW Arizona, USA. J. Struct. Geol. 21, 313–321.
Ó Cofaigh, C., Evans, J., Dowdeswell, J.A., Larter, R., 2007. Till characteristics, genesis and transport beneath Antarctic paleo-ice streams. J. Geophys. Res. 112, F03006.
Palmer, A.P., 2005. The Micromorphological Description, Interpretation and Palaeoenvironmental Significance of Lacustrine Clastic Laminated Sediments. Unpublished PhD thesis, University of London.
Passchier, C.W., Trouw, R.A.J., 1996. Microtectonics. Springer.
Phillips, E.R., Auton, C.A., 2000. Micromorphological evidence for polyphase deformation of glaciolacustrine sediments from Strathspey, Scotland. In: Maltman, A.J., Hubbard, B., Hambrey, M.J. (Eds.), Deformation of Glacial Materials, vol. 176. The Geological Society of London, Special Publication, pp. 279–291.
Phillips, E., Merritt, J., 2008. Evidence for multiphase water-escape during rafting of shelly marine sediments at Clava, Inverness-shire, NE Scotland. Quat. Sci. Rev. 27, 988–1011.
Phillips, E., Evans, D.J.A., 2019. Synsedimentary glacitectonic deformation within a glacilacustrine-esker sequence, Teesdale, Northern England. PGA (Proc. Geol. Assoc.) 130, 624–649.
Phillips, E., Hughes, L., 2014. Hydrofracturing in response to the development of an overpressurised subglacial meltwater system during drumlin formation: an example from Anglesey, NW Wales. PGA (Proc. Geol. Assoc.) 125, 296–311.
Phillips, E.R., Kearsey, T., 2020. Mass flow and hydrofracturing during Late Devensian moraine emplacement, NE Scotland. PGA (Proc. Geol. Assoc.) 131, 730–750.
Phillips, E., Lee, J.R., 2011. Description, measurement and analysis of glacitectonically deformed sequences. In: Phillips, E., Lee, J.R., Evans, H.M. (Eds.), 2011. Glacitectonics – Field Guide. Quaternary Research Association.
Phillips, E.R., van der Meer, J.J.M., Ferguson, A., 2011. A new 'microstructural mapping' methodology for the identification and analysis of microfabrics within glacial sediments. Quat. Sci. Rev. 30, 2570–2596.
Phillips, E.R., Lipka, E., van der Meer, J.J.M., 2013. Micromorphological evidence of liquefaction and sediment deposition during basal sliding of glaciers. Quat. Sci. Rev. 81, 114–137.
Phillips, E., Evans, D.J.A., van der Meer, J.J.M., Lee, J.R., 2018a. Microscale evidence of liquefaction and its potential triggers during soft-bed deformation within subglacial traction tills. Quat. Sci. Rev. 181, 123–143.
Phillips, E., Spagnolo, M., Alasdair, C.J., Pilmer, A.C.J., Rea, B.R., Piotrowski, J.A., Ely, J.C., Carr, S., 2018b. Progressive ductile shearing during till accretion within the deforming bed of a palaeo-ice stream. Quat. Sci. Rev. 193, 1–23.
Phillips, E., Carter, G., Teasdale, D., 2022. Microscale evidence of the role of water during the emplacement of mass flows in glacial environments. Q. J. Eng. Geol. Hydrogeol. 55, 2021–2026.
Piotrowski, J.A., Tulaczyk, S., 1999. Subglacial conditions under the last ice sheet in northwest Germany: ice-bed separation and enhanced basal sliding? Quat. Sci. Rev. 18, 737–751.
Piotrowski, J.A., Mickelson, D.M., Tulaczyk, S., Krzyszowski, D., Junge, F., 2001. Were subglacial deforming beds beneath past ice sheets really widespread? Quat. Int. 86, 139–150.
Piotrowski, J.A., Larsen, N.K., Junge, F., 2004. Soft subglacial beds: a mosaic of deforming and stable spots. Quat. Sci. Rev. 23, 993–1000.
Piotrowski, J.A., Larsen, N.K., Menzies, J., Wysota, W., 2006. Formation of subglacial till under transient bed conditions: deposition, deformation, and basal decoupling under a Weichselian ice sheet lobe, central Poland. Sedimentology 53, 83–106.
Przybylski, B., 2008. Geomorphic traces of a Weichselian ice stream in the Wielkopolska Lowland, western Poland. Boreas 37, 286–296.
Punkari, M., 1997. Glacial and glaciofluvial deposits in the interlobate areas of the Scandinavian ice sheet. Quat. Sci. Rev. 16, 741–753.
Schlegel, R., Murray, T., Smith, A.M., Brisbourne, A.M., Booth, A.D., King, E.C., Clark, R.A., 2022. Radar derived subglacial properties and landforms beneath rutford ice stream, west Antarctica. J. Geophys. Res.: Earth Surf. 127, e2021JF006349. https://doi.org/10.1029/2021JF006349.
Shumway, J.R., Iverson, N.R., 2009. Magnetic fabrics of the Douglas till of the Superior lobe: exploring bed-deformation kinematics. Quat. Sci. Rev. 28, 107–119.
Spagnolo, M., Phillips, E., Piotrowski, J.A., Rea, B.R., Clark, C.D., Stokes, C.R., Carr, S.J., Ely, J.C., Ribolini, A., Wysota, W., Szuman, I., 2016. Ice stream motion facilitated by a shallow-deforming and accreting bed. Nat. Commun. 7, 10723. https://doi.org/10.1038/ncomms10723.
Stokes, C.R., Clark, C.D., 2001. Palaeo-ice streams. Quat. Sci. Rev. 20, 1437–1457.
Szuman, I., Kalita, J.Z., Ewertowski, M.W., Clark, C.D., Livingstone, S.J., Kasprzak, L., 2021. GIS dataset: geomorphological record of terrestrial-terminating ice streams, southern sector of the Baltic Ice Stream Complex, last Scandinavian Ice Sheet, Poland. Earth Syst. Sci. Data 13, 4635–4651. https://doi.org/10.5194/essd-13-4635-2021.
Thomason, J.F., Iverson, N.R., 2006. Microfabric and micro-shear evolution in deformed till. Quat. Sci. Rev. 25, 1027–1038.
Trommelen, M.S., Ross, M., Campbell, J.E., 2012. Glacial terrain zone analysis of a fragmented paleoglaciologic record, southeast Keewatin sector of the Laurentide Ice Sheet. Quat. Sci. Rev. 40, 1–20.
Tulaczyk, S., Kamb, B., Scherer, R.P., Engelhardt, H.F., 1998. Sedimentary processes at the base of a West Antarctic ice stream: constraints from textural and compositional properties of subglacial debris. J. Sediment. Res. 68, 487–496.
Tulaczyk, S.M., Kamb, B., Engelhardt, H., 2000. Basal mechanics of ice stream B: I. Till mechanics. J. Geophys. Res. 105, 463–481.
Tylmann, K., Piotrowski, J.A., Wysota, W., 2013. The ice/bed interface mosaic: deforming spots intervening with stable areas under the fringe of the Scandinavian Ice Sheet at Sampława, Poland. Boreas 42, 428–441. https://doi.org/10.1111/j.1502-3885.2012.00294.x.
Vaughan-Hirsch, D.P., Phillips, E., Lee, J.R., Hart, J.K., 2013. Micromorphological analysis of poly-phase deformation associated with the transport and emplacement of glaciotectonic rafts at West Runton, north Norfolk, UK. Boreas 42, 376–394.
van der Wateren, F.M., Kluiving, S.J., Bartek, L.R., 2000. Kinematic indicators of subglacial shearing. In: Maltman, A.J., Hubbard, B., Hambrey, M.J. (Eds.), Deformation of Glacial Materials, vol. 176. Geological Society of London, Special Publication, pp. 259–278.
Williams, M.L., Scheltema, K.E., Jercinovic, M.J., 2001. High-resolution compositional mapping of matrix phases: implications for mass transfer during crenulation cleavage development in the Moretown Formation, western Massachusetts. J. Struct. Geol. 23, 923–939.